Title	Instrumented concrete pile tests – part 1: a review of instrumentation and procedures
Author(s)	Flynn, Kevin N.; McCabe, Bryan A.
Publication Date	2021-11-03
Publication Information	Flynn, Kevin N., & McCabe, Bryan A. (2022). Instrumented concrete pile tests – part 1: a review of instrumentation and procedures. Proceedings of the Institution of Civil Engineers - Geotechnical Engineering, 175(1), 86-111. doi:10.1680/jgeen.21.00126
Publisher	ICE Publishing
Link to publisher's version	https://doi.org/10.1680/jgeen.21.00126
Item record	http://hdl.handle.net/10379/17132
DOI	http://dx.doi.org/10.1680/jgeen.21.00126

Instrumented Concrete Pile Tests – Part 1: A Review of Instrumentation and Procedures

Kevin N. Flynn BA BAI PhD CEng MIEI, Principal Geotechnical Engineer, AGL Consulting Geotechnical Engineers, Sandyford, Dublin 18, Ireland.

Bryan A. McCabe BA BAI PhD CEng FIEI, Senior Lecturer, School of Engineering, National University of Ireland, Galway, Ireland.

E-mail: bryan.mccabe@nuigalway.ie

ABSTRACT:

Preliminary pile tests are becoming increasingly routine in piling projects, some of which are instrumented to help optimise parameters for working pile design. However, the execution of a successful test on an instrumented concrete pile is not straight-forward; practitioners are often faced with difficulties in interpreting the results from the instrumentation due to factors such as installation and curing effects, insufficient and/or malfunctioned gauges and testing procedures. This paper provides a detailed methodology for the successful execution of an instrumented pile test addressing all of these factors. Established and emerging trends in instrumented concrete pile testing are captured through a database of over 100 published case histories from the literature. It is envisaged that the methodologies described in this paper, together with the companion paper on strain interpretation, can provide the practitioner with a helpful guide to enable a successful instrumented concrete pile test.

KEYWORDS: cast in situ, concrete, piles, installation, curing, load test, instrumentation, strain

INTRODUCTION

Preliminary pile tests are becoming increasingly commonplace in European piling projects, exploiting the design benefits of reduced partial factors available by pile testing, in accordance with Eurocode 7 (CEN, 2004). Furthermore, cost-effective instrumentation can be capitalised upon in preliminary piles to derive the shaft resistance distribution and base resistance mobilised during static loading, in order to optimise pile designs. However, instrumented concrete pile tests are not simple to perform and their interpretation involves careful consideration of several factors, including the type, position and orientation of strain gauges, the effects of installation and curing, and static load test procedures. The decision-making process associated with these factors is considered in detail in this paper, in the context of current and emerging trends in instrumented pile testing, captured through a database of over 100 case histories from the literature. It is envisaged that the methodologies described in this paper, together with the companion paper by Flynn and McCabe (2021) on strain interpretation, can provide the practitioner with the means of executing successful instrumented concrete pile tests.

PILE INSTRUMENTATION

The magnitude of load (P) in an instrumented concrete pile is determined as follows:

$$P = E_{pile}A_{pile}\varepsilon_{elastic} \qquad (1)$$

where E_{pile} is the pile modulus, A_{pile} is the pile cross-sectional area and $\varepsilon_{elastic}$ is the mobilised elastic mechanical strain. Appropriate instrumentation is necessary to measure strain accurately (and infer axial load using Equation 1). This section provides an overview of the types and typical arrangements of strain gauges used in concrete piles, as deduced from an instrumented pile database. Table 1 summarises the scope of the database, with full details of the individual piles in Table 2.

Instrumentation Types

The typical types of instrumentation used in both precast and cast-in-situ concrete piles are, progressing from older to newer technologies, (i) electrical resistance gauges, (ii) vibrating wire gauges and (iii) fibre optic sensors. A comparison of these types, including typical strain range, resolution, and advantages and limitations for use in concrete piles, is presented in Table 3. All strain gauges in concrete piles operate on the principle of strain compatibility, whereby the strain measured by the gauge is assumed to be equal to the strain in the surrounding concrete. Such an assumption is valid, provided no cracking occurs within the pile concrete at the gauge level.

Electrical resistance

Electrical resistance strain gauges (ERSG) are perhaps the simplest and most cost-effective type for determining strain in structural members. The gauges, which have typical lengths of 5 to 15 mm, are mounted directly on the surface of a structural member (Figure 1a). When contraction or expansion occurs, the corresponding change in length across the gauge results in a proportional change in electrical resistance. This change in resistance can be calibrated against known applied strains using a gauge factor, allowing the change in strain to be quantified as follows:

$$\varepsilon_{total} = \frac{\Delta R}{R_0} \times GF_{ER} \tag{2}$$

where ε_{total} is the measured (total) strain, ΔR is the change in resistance, R_0 is the initial resistance and GF_{ER} is the electrical resistance gauge factor. ERSGs are typically configured in a full Wheatstone bridge circuit to minimise the effects of temperature and eccentricities due to bending within the structural member at the gauge location. Bonded foil and weldable electrical resistance gauges are considered the most suitable for use in concrete piles (Dunnicliff, 1988).

The preparation of ERSGs is more labour intensive than other gauge types and is usually performed in a laboratory prior to site mobilisation. For cast-in-situ piles, the gauges are usually applied directly to the surface of the pile reinforcement. Alternatively, the gauges may be applied to an independent ‘sister bar’, as shown in Figure 2. This comprises a 0.5 to 1.0 m long steel bar with the gauge encapsulated within the central section. The overall length of the sister bar allows it to be mounted to the internal face of the transverse shear links between the main longitudinal reinforcement bars.

Prior to gauge installation, the surface of the steel bar is smoothened by polishing and cleaned using a solvent. The gauge is then applied to the surface using adhesive, with the lead wires for connection to the data acquisition unit attached by soldering. Protection from damage and moisture ingress (which can lead to erroneous outputs) is provided by encapsulating the gauge in an epoxy adhesive coating; this is a critical element in the preparation process, as the gauge will be immersed in fluid concrete during casting.

ERSGs enable high frequency sampling rates, making them ideal for use in piles subjected to dynamic load testing (Brown, 2002; Brown and Hyde, 2008; Robertson and Muchard 2007). Nie et al. (2016) also reported the successful use of these gauges in high-strength precast concrete pipe piles where space limitations prevented the use of vibrating wire strain gauges. Despite these advantages, ERSGs accounted for only 20 of the 117 case histories in the pile test database in Table 2.

Vibrating wire

Vibrating wire strains gauges (VWSG) are currently the most popular gauge choice for instrumented concrete piles in practice, and were deployed in 79% of the case histories in Table 2. A steel wire is tensioned between two mounting blocks housed within a protective casing and sleeve which in turn is welded to steel bars (Figure 1b) or metal flanges at each end (Figure 1c). A magnetic field, generated by electromagnetic coils within the casing, is used to oscillate the steel wire at its resonant frequency. This process generates an alternating current, the frequency of which is recorded by a datalogger connected to the gauges. A change in load within the pile at the gauge level results in a proportional change in length (and hence frequency) of the wire, enabling the change in strain to be derived using the following equation:

$$\varepsilon_{total} = (f_1^2 - f_0^2) \times GF_{VW} \quad (3)$$

where f_0 and f_1 are the initial and current frequency readings respectively and GF_{VW} is the vibrating wire gauge factor determined in manufacturer's calibration tests. As the steel wire is also influenced by changes in temperature, each gauge is typically fitted with a thermistor within the protective housing to enable thermal strains to be ascertained.

The main types of VWSG suitable for use in concrete piles are (i) sister bars and (ii) embedment gauges. The sister bar gauge is analogous to that previously described for ERSGs; the strain gauge is encapsulated with a protective sleeve which in turn is welded to steel rebar at each end (Figure 3a). The overall length of the sister bar (0.5 to 1.0 m) allows it to be attached to the inner face of helical links on the reinforcement cage (Figure 4a). A reduced-length sister bar can also be utilised where a gauge is required in close proximity to the base of a pile; in this instance, circular steel flanges are attached to the ends of the bar to ensure sufficient fixity of the gauge within the concrete (Figure 3b).

A typical vibrating wire embedment gauge is shown in Figures 1a and 4b. The length of this gauge type (≈ 100 to 150 mm) prevents direct attachment to shear reinforcement, resulting in the need to 'embed' the gauge directly within the concrete. This is achieved using wooden mounting blocks which in turn are tied to the internal face of the main reinforcement bars (Figure 4b); alternatively, transverse steel ties can be welded to the reinforcement cage to provide a suitable anchoring point for the gauges (Figure 4c).

Three of the case histories in Table 2 used a combination of embedment and sister bar VWSGs in instrumented concrete piles. Unfortunately, the comparative performance of these gauge types (due to the variable gauge lengths) was not presented in these studies. Such comparisons would be helpful, given that the unit cost of an embedment gauge is typically less than a sister bar. However, Hayes and Simmonds (2002) note that the length of a sister bar VWSG makes it less vulnerable to local defects within the concrete (e.g. cracking, fissures or air voids) compared to the embedment type (which have a gauge length in the order of 100 to 150 mm).

VWSGs have a typical strain range of 3000 to 5000 $\mu\varepsilon$ which is predicated upon the level of pre-tension induced in the steel wire between the mounting blocks in the casing (although some manufacturers allow the level of pre-strain to be adjusted by the user). VWSGs can transmit frequencies over significant cable lengths without degradation from resistances due to temperature fluctuations, contact and water ingress (Hayes and Simmonds, 2002; Webb and Viswanathan, 2005), making them suitable for use in long-term monitoring of pile behaviour. Whilst VWSGs have traditionally been considered unsuitable for measuring strain in concrete piles during dynamic events (e.g. pile driving and cyclic load tests) due to the limitations in the rate of sampling (Dunnicliff, 1988), dataloggers capable of high frequency strain monitoring are now commercially available (e.g. Campbell Scientific, 2020).

Fibre optics

The newest of the three instrumentation types considered herein, fibre optic strain sensors (FOSS) have the ability to overcome many of the limitations of ERSGs and VWSGs due to their lightweight construction, ease of installation, resistance to corrosion, immunity from electromagnetic interference and long-term stability, making them ideal for use in concrete piles (de Battista and Kechavarzi, 2021). A typical optical fibre, shown in Figure 5a, comprises a silica glass core in which the light is transported, a silica glass cladding surround (with a lower refractive index to confine light to within the core), followed by a polymer buffer coating to protect the fibre. The diameters of the core, cladding and buffer are typically 9 to 62.5 µm, 125 µm and 250 µm respectively. Further details of the properties of optical fibres are presented in Kechavarzi et al. (2016).

Fibre optic sensors are typically categorised into:

(i) Discrete types where the primary role of the fibre optic cable is to transfer light to and from a discrete sensor (which makes use of the properties of the light to measure strain)

(ii) Distributed fibre optic sensing (DFOS), in which the fibre optic cable itself acts as the strain sensor throughout its length.

Variants of discrete sensors include fibre Bragg gratings (FBG) and interferometric fibre optic sensors (IFOS). FBGs comprise a prefabricated grating within the core of an optical fibre of the sensor (Figure 5c) that induces a periodic variation in refractive index to reflect light centred about the Bragg wavelength, λ_B. When the sensor experiences a change in strain (due to mechanical and/or thermal effects), the Bragg wavelength undergoes a corresponding change in wavelength $\Delta\lambda_B$ which can be correlated to strain. Correction for thermal-related strain requires knowledge of the thermal properties of the optical fibre within the sensor (Kister et al. 2007). IFOS determine the magnitude of strain by assessing the interference resulting from two beams propagated along different optical paths within the fibre (Figure 5d), enabling high accuracy and sensitivity in strain measurement to be achieved over a wide dynamic range (Lee et al. 2012). Variants of IFOS sensors include extrinsic Fabry-Perot interferometers or EFPI (Schilder et al. 2013) which have very short gauge lengths (5 to 10mm) and Surveillance d'Ouvrages par Fibres Optiques or SOFO® which have active sensor lengths ranging from 0.25 to 10 m (Glisic et al. 2002).

FBG sensors enable use of a single fibre optic cable to connect multiple sensors in a process known as 'multiplexing' (Kister et al. 2007) and hence are sometimes referred to as 'quasi-distributed' sensors. The short gauge length of FBGs and EFPIs allows the sensors to measure strain at a high resolution, but also makes them vulnerable to local strain anomalies at the sensor location (e.g. cracking or voids in the concrete) in comparison to other types. Issues with bandwidth within the fibre optic cable may arise when multiplexing as the number of sensors increases (Soga and Luo, 2018). The unit cost of a FBG sensor is also comparable to a VWSG (Klar et al. 2006) and hence, the number of sensor levels will depend on the budget for the instrumented pile test.

In distributed fibre optic sensing (DFOS), the emission of light through the fibre core results in scattering of light waves in all directions at different wavelengths. Differences in the properties of back-scattered light (due to strain and/or temperature in the fibre) is recorded by an optical spectrum analyser and analysed by appropriate software programs to produce a continuous profile of strain and temperature along the fibre. The following methods of analysis for DFOS systems have been utilised for instrumented concrete piles in Table 2:

- Optical Frequency-Domain Reflectometry (OFDR)
- Brillouin Optical Time-Domain Analysis (BOTDA)
- Brillouin Optical Time-Domain Reflectometry (BOTDR)

Rayleigh scattering of the light is used in OFDR to obtain measurements of strain and temperature along the fibre. A pulse of light (referred to as the signal light) is emitted through one end of the fibre using the optical spectrum analyser (Figure 5e). Natural impurities within the fibre core result in Rayleigh scattering as the signal light travels down the fibre, with back-scattered Rayleigh light received by the analyser. Interference between back-scattered and reference light (obtained independent of the test fibre by reflection of the signal light using a fixed mirror within the analyser) enables the Rayleigh spectral shift to be determined. By comparing the measured shift with the initial condition (Bersan et al. 2018), the differences can be correlated to strain and/or temperature changes, enabling continuous profiles along the fibre to be obtained.

BOTDA and BOTDR methods are based on Brillouin scattering of light within an optical fibre. The interaction between the incident light and propagating density waves or acoustic photons results in scattering of light at a shifted frequency, referred to as the Brillouin frequency shift, which is approximately 10 to 11 GHz at a wavelength of 1550 nm for the incident light (Soga and Luo, 2018). Subjecting the fibre to a change in length (due to temperature and/or strain) results in a proportional shift in the Brillouin frequency. In BOTDA, light is emitted from both ends of the fibre (comprising a short pump pulse at one end and a continuous wave at the other – see Figure 5f), resulting in the generation of an acoustic wave which alters the properties of the fibre (in a process known as stimulated Brillouin scatter). The effect of strain and temperature is then determined by assessing the loss or gain in the Brillouin frequency arising from the power transfer between the two light sources. BOTDR is based on spontaneous Brillouin scatter whereby the emission of a pulse of light form one end of the fibre results in Brillouin scatter that is insufficient to alter the fibre properties (Figure 5g). By recording the frequency of the back-scattered light, the shift in peak Brillouin frequency can be analysed to determine the magnitude of strain and temperature (Klar et al. 2006).

The distinct advantage of DFOS in comparison to other types of instrumentation is the ability to obtain continuous measurements of strain and/or temperature along the full length of a concrete pile, allowing localised defects in the concrete to be identified which could otherwise be missed using discrete instrumentation. However, as highlighted in Table 3, each DFOS method has specific advantages and disadvantages which need to be considered for instrumented concrete piles. For example, the spatial resolution of BOTDA and BOTDR is in the order of 0.5 to 1.0 m at every 0.05 m length of cable (Klar et al. 2006), whereas OFDR provides a spatial resolution in the order of 10 mm (Bersan et al. 2018). However, OFDR is typically limited to cable lengths of 30 m or less, whereas BOTDA and BOTDR can provide measurements over much longer distances (up to 50 km). BOTDA relies on the interaction of light emitted from both ends of a fibre and hence will be compromised by damage to the cable. On the other hand, BOTDR only requires access at one end of the fibre, with a looped cable providing an additional level of redundancy in the event that the cable is damaged (Kechavarzi et al., 2016). Given that optical fibres register a combination of mechanical and thermal strain, an additional temperature-sensing cable (which is isolated from mechanical strain) is required to remove the thermal strain component from the combined strain measurement. This is typically achieved by isolating the fibre within a gel-filled sheath (Figure 5b). Further guidance on correction for thermal strain in concrete piles using DFOS is presented by Mohamad et al. (2014).

The installation process for fibre optic cables, illustrated in Figure 6, involves either clamping or bonding the cables to the main reinforcement bars (usually in pairs orientated at 180º) along the full pile length (e.g. de Battista et al. 2016; Kister et al. 2007; Pelecanos et al. 2017). For DFOS systems, the strain-sensing fibre cables are typically pre-tensioned to between 1500 and 3000 $\mu\varepsilon$ prior to casting (to minimise issues with signal interpretation in loose cables), whereas temperature cables are usually attached in a non-taut configuration. Readers are referred to Kechavarzi et al. (2016) for a comprehensive guide to the installation of fibre optic cables.

GAUGE ARRANGEMENTS

Gauge levels

For discrete instrumentation types, the next step in the instrumentation process is to determine the number of gauge levels in the pile. The most basic form of instrumented pile test involves separation of the total pile resistance into the respective shaft and base resistances only, accomplished using two levels of strain gauges, one at the head (for establishing the relationship between pile modulus and strain, see Flynn and McCabe, 2021) and the other as close to the pile base as possible (Figure 7a). This approach provides no information on the shear stress variation along the pile shaft which is unhelpful where layered stratigraphy is present.

The use of multiple strain gauge levels between the pile head and base will provide more comprehensive information on the shear stress variation along the embedded length (Figure 7b). Where an instrumented concrete pile is installed in layered stratigraphy (Figure 7c), the gauge levels should be placed at the interfaces between layers. In this instance, is it crucial to determine the ground conditions accurately at or as close as possible to the pile position, as any deviations in stratigraphy from that assumed may compromise the reliability of the strain interpretation process. The continuous profiling offered by cone penetration testing (CPT) is ideal in this regard, and the cone end resistances measured also enable a comparison of the normalised shaft and base resistances derived with those reported in the literature (e.g., Gavin et al., 2013; Lehane et al., 2005).

Where cast-in-situ piles are constructed through very soft fine-grained soils into underlying soils of higher strength (e.g. hard clays, dense sands and gravels or rock), concrete over-supply within the weaker layer can result in significant deviations from the nominal pile diameter assumed in the strain interpretation process. If a gauge is placed at a depth corresponding to this layer, the enlarged cross-section will result in an apparent reduction in strain (due to the larger axial rigidity EA component in Equation 1) at this level (Figure 7c), which may be misinterpreted as additional shaft resistance. Similarly, where bored piles are drilled through overburden into rock, a reduction in pile diameter will inevitably occur due to the differences in the diameter of casings in the overburden and drilling tools in the rock. The placement of strain gauges across this interface may again result in the shaft resistance being over-estimated due to the additional end-bearing resistance created at the soil/rock interface by the larger pile diameter within the overburden (Figure 7d).

The uppermost gauge level is typically used to derive the correct strain-dependent pile modulus as part of the strain interpretation process. Unfortunately, the selection of an appropriate level is not straightforward. The generation of resistance between pile head and uppermost gauges, e.g. due to shaft friction and/or end-bearing resistance on the underside of the pile cap, can lead to significant errors in the strain interpretation process. This risk can be mitigated using compressible high-density polystyrene on the underside of the pile cap, as reported by Unwin and Jessep (2004). Alternatively, local excavation of the soil surrounding and immediately beneath the pile cap could be considered.

The application of axial load on the pile cap may result in non-uniform stresses near the pile head due to end-effects. As such, for discrete instrumentation, the uppermost level should be placed at a distance at least three times the pile diameter, D, below the pile head, in accordance with St. Venant's Principle (Batten et al., 1999; Lam and Jefferis, 2011). However, the uppermost level of the case histories in Table 2 varied from 0 to 17 D, with mean and median values of 2.8 D and 1.7 D, respectively, and the choice of level is likely to be influenced by factors such as pile length, pile cap embedment, temporary casing/sleeving and ground conditions.

The lowermost level for discrete gauge types should as close to the base as possible in order to accurately determine the base resistance during loading. Again, distances reported in the literature in this regard range from 0 to 11.2 D, with mean and median distances of 1.5 D and D, respectively. As noted previously, the length of a traditional sister bar gauge will prevent its placement within 0.5 m of the base; this can be alleviated by selecting reduced-length sister bars with end flanges or else by using embedded strain gauges. Unfortunately, placement of strain gauges too close to the base of the cage will increase the risk of over-stressing and damage during installation, particularly where the cage is plunged after concreting.

Gauge Orientation

The instrumented pile database (Table 2) identified the following typical instrumentation configurations, illustrated in Figure 8:

(i) A single gauge in the centre of the pile.

(ii) Two gauges placed diametrically (180°) apart on either the main or shear reinforcement.

(iii) Three gauges orientated at 120°.

(iv) Four gauges, comprising two pairs of gauges placed at 90° to each other.

The use of a single gauge per level is generally limited to micropiles, in which strain gauges are typically spot-welded directly to a central reinforcement bar. However, a single strain gauge per level provides no redundancy in the event of gauge malfunction during installation, curing and/or loading.

Whilst multiple gauges per level are primarily chosen for redundancy purposes, they also serve to minimise the influence of pile bending during loading on the measured strain. This phenomenon results from inevitable eccentricities in the applied axial load which can be significant in certain circumstances. Significant variations in mobilised strain in individual sensors in the upper portions of instrumented piles under compression load were reported by Bersan et al. (2018) and Kania and Katoka Sørensen (2018), both of whom used DFOS systems. Inspection of the ground profiles presented in these studies suggests that poor confinement from the surrounding soil promoted lateral deflection of the pile head as the eccentric load was applied, leading to the aforementioned deviations in strain.

Multiple strain gauges were used per level in the majority of case histories in Table 2. Of these, 50% of studies used pairs of gauges orientated at 180^{o} to each other, 14% had three gauges at intervals of 120^{o}, while 28% utilised two pairs of gauges placed at right angles to one another. The use of two gauges allows instrumentation costs to be minimised; however, should a gauge malfunction, the strain reading from the sole remaining gauge will be affected by bending (the extent of which can no longer be quantified) and should be treated with extreme caution when interpreting the test results (Siegel, 2010; Fellenius and Tan, 2012). Practitioners may be tempted to use three gauges arranged at angles of 120^{o} to provide additional redundancy; however, in the event of a gauge malfunction, the average of the remaining gauges still cannot compensate for bending effects, as the gauges are not orientated at 180^{o} to one another (Sinnreich, 2021). As such, two pairs of gauges located at 90^{o} to each other provides the most reliable strain gauge arrangement. As demonstrated by Flynn and McCabe (2021), the influence of bending is most significant near the head of a concrete pile under compression loading and hence, there may be scope to reduce the instrumentation arrangement to 2 No. gauges at 180^{o} at sections of the pile where the effects of bending are minimal. In fact, such gauge arrangements have been utilised in several studies involving instrumented concrete piles (e.g. Hai and Dai (2013), Kim et al. (2004) Mullins et al. (2003) and Vipulanandan et al. (2012)).

INSTALLATION

For precast piles, the process of instrumenting the reinforcement is performed during pile construction in the casting yard, whereas installation of instrumentation for cast-in-situ types is normally carried out on site due to the risk of gauge damage during transportation of an instrumented cage from an off-site location.

For cast-in-situ piles, the instrumented cage must be carefully lifted into a vertical position for insertion into the ground. The reinforcement cage for a bored pile is usually installed in the bore prior to casting (requiring the use of a tremie pipe to prevent damage to the gauges), whereas for CFA, DCIS and other cast-in-situ types such as micropiles, the instrumented cage must be plunged into the freshly-cast concrete. The cage is usually plunged under its self-weight; where refusal occurs, the cage can be pushed to the base of the pile using an excavator bucket. For excessively long piles (typically greater than 14m embedment), the use of a low-frequency vibrator may be considered, exercising extreme caution due to the risk of disturbance and damage to the gauges. The installation process can be challenging for the following reasons:

(i) The use of high strength concrete grades can result in the mix hardening prematurely, leading to premature refusal of the reinforcement cage. This may be mitigated somewhat by using a mix with ground granulated blast furnace slag (GGBS) to achieve slower early strength gain or plasticizers to improve workability.

(ii) The large compression forces in a preliminary test typically require the pile to be heavily reinforced; the resulting congestion of steel can restrict concrete flow during cage insertion.

(iii) A loss in verticality of the cage during plunging, particularly in thick layers of soft compressible soil, can prevent insertion of the cage into an underlying stiffer stratum. Flynn (2014) describes such a problem with a DCIS pile constructed through over 8 m of very soft to soft alluvial clays into underlying dense gravels. The loss of verticality resulted in the base of the cage coming in contact the sides of the gravel socket and damaging several strain gauges in the lower section of the cage.

Following completion of concreting and installation of reinforcement, a concrete pile cap is constructed at the head of each test pile for load application and to accommodate the egress of instrumentation cables through the side. The cap must be sufficiently reinforced to prevent bursting stresses resulting in premature termination of the test and curtailing the benefits of the instrumentation. Consideration should also be given to the dimensions of the pile cap; circular caps formed using steel casing are typically utilised (Figure 9a), although square pile caps may be preferable where several hydraulic jacks are required to apply large loads to the pile (Figure 9b).

Several of the case histories in Table 2 used temporary steel or plastic casings to minimise the shaft resistance of bored piles during loading. The use of double-sleeved casings, described by Zhan and Yin (2000), isolates the ground from the pile using an enlarged outer diameter casing, with the pile cast within an inner casing (Figure 10a). To restrict lateral movement of the pile during loading, the annulus between the casings is typically filled with a low strength cement-bentonite grout. Where a reduction in base resistance during loading is desired (e.g. to facilitate higher applied loads for mobilising shaft resistance), consideration can be given to the use of compressible high-density polystyrene to create a soft toe at the base of bored piles, as successfully implemented for an instrumented bored pile undertaken by AGL Consulting (Figure 10b). An alternative method reported by Unwin and Jessep (2004) involves placing a water-filled polyurethane bag at the base of the bore.

CURING AND RESIDUAL LOADS

Unlike preformed piles, cast-in-situ piles must cure in the ground and will therefore undergo changes in volume as the concrete sets and cures. Moreover, the installation of a pile, regardless of type, will disturb the surrounding soil (from lateral or vertical soil movements) and the excess pore pressures generated in cohesive soils will induce downdrag on the pile as they dissipate (Fellenius, 2002). Therefore, the assumption of a load-free pile as the initial condition for a load test is questionable. A limited number of recent studies have considered the processes which occur within the concrete and soil after the installation of a cast-in-situ pile to gain a better understanding of residual load development. The scope of these tests is summarised in Table 4, which includes details of pile type, pile dimensions, instrumentation used and duration of curing, and highlights the individual processes for which measurements were made within the concrete and soil. The level of detail in these studies varies from basic two-point tests (i.e. strains recorded immediately post-installation and just before the load test) to more detailed studies in which strain and temperature were monitored over part or all of this period. This section provides commentary on each process in terms of strain and temperature (where relevant), as these can be measured using the instrumentation incorporated in the pile prior to casting.

Initial concrete set and hydration

Once a concrete pile is constructed, the mixture of the cement binder and water results in an exothermic chemical reaction. The level of heat generated during hydration varies with the properties of the binder and the insulating medium outside the pile. In the case of a precast pile, the insulating material prior to installation is air (once the formwork is stripped) which is a poor insulator, so the heat generated dissipates quickly. In the case of a cast-in-situ pile, the process is prolonged as soil is a superior insulator. As the reaction proceeds, the hydration temperatures will continue to rise for several hours after casting, and the concrete will begin to harden or 'set' during this period (Figure 11a). Initial set is assumed to be complete at peak temperature T_{peak} (Neville and Brooks, 1987).

The authors have compiled temperature data from relevant case histories in Table 4 (as well as unpublished records from the first author) to investigate hydration temperature behaviour during initial set and curing. Only hydration temperature profiles at or close to the mid-depth of each pile were used in the study, as temperatures at the distal pile sections are likely to be influenced by three-dimensional effects. On this basis, data from 19 piles were collated for initial set. The resulting variation in T_{peak} with pile diameter, D, is presented in Figure 12a where no correlation is apparent; this is to be expected however, as the absolute hydration temperature is likely to be influenced by factors such as concrete mix, ground temperatures, construction methods and gauge position within the pile cross-section. However, when the time to peak temperature t_{peak} is plotted against D in Figure 12b, a near-linear relationship is obtained (although several piles in the dataset with diameters between 0.5 and 1.0 m have t_{peak} values which are greater than the overall linear trend). Figure 12b serves as a useful first-order approximation for estimating the time to peak temperature t_{peak} (and hence initial set) when assessing residual load development methods, as discussed by Flynn and McCabe (2021).

The case histories in Table 4 where strain behaviour was reported during initial set and hydration were noted to be conflicting. Several studies (Pennington 1995, Siegel and McGillivray 2009, Fellenius et al. 2009 and Lam and Jefferis 2011) did not attempt to correct for thermal strain during this phase and hence reported measured or 'total' strain ε_{total}. As the hydration temperatures increased, compressive ε_{total} values were observed in these studies. Such observations conflict with the expectation that a rise in temperature will cause thermal expansion of a pile. Hence, correction for thermal strains is warranted. The level of thermal strain $\varepsilon_{thermal}$ present in a pile at a particular instance after casting can be determined using Equation 4:

$$\varepsilon_{thermal} = \alpha \Delta T = \alpha(T - T_0) \quad (4)$$

where α is the coefficient of thermal expansion of the material in question, ΔT is the change in temperature, T_0 is the initial temperature and T is the current temperature. The 'mechanical' strain ε_{mech} during initial set and hydration can be inferred as follows:

$$\varepsilon_{mech} = \varepsilon_{total} - \varepsilon_{thermal} \quad (5)$$

The majority of studies in Table 4 used VSWGs to measure axial strains during the curing process. Given that these gauges comprise a pretensioned steel wire, the α value in Equation 4 is assumed to be that of steel (i.e. ≈ 12 με/°C). Using Equations 4 and 5 with α =12 με/°C resulted in ε_{mech} values which were tensile at peak temperature in the studies by Farrell and Lawler (2008) and Pennington

(1995), which is in line with expectations for pile behaviour at peak temperature discussed above and in agreement with the tensile strain response during initial set of a 1.5m diameter bored pile in London, UK reported by Kister et al. (2007) using FBG sensors. Given that the studies in which the uncorrected compressive strains were reported during initial set were obtained using VWSGs, the compressive ε_{total} measurements are most likely explained by the tensioned steel wire within the gauge casing expanding at a greater rate ($\alpha \approx 12$ με/°C) than the surrounding casing (which is bonded to the concrete with $\alpha \approx 7$ to 10 με/°C) during the hydration process, resulting in an 'apparent' compression strain as the wire slackens (Bicocchi 2011; Fellenius et al. 2009; McCartney and Murphy, 2012).

Curing and strength development

After hydration temperatures have peaked, the pile will experience a gradual reduction in temperature with time. The durations for full decay of hydration temperatures to ambient $T_{ambient}$ for the studies in Table 4 were typically 8-10 days, although a period of 30 days was required for temperatures to stabilise within a 2.6 m diameter bored pile in Vancouver, Canada (Fellenius et al., 2009). The authors have used relevant temperature data from the studies in Table 4 to produce Figure 12(c) which shows that the time taken for 90% dissipation in hydration temperatures, t_{90}, i.e. from T_{peak} to $T_{ambient}+0.1(T_{peak}-T_{ambient})$, is a function of square of the pile diameter, D^2, in a similar manner to the dissipation of excess pore pressures following driven pile installation. Note that only 15 of the studies represented in Figures 12(a) and (b) could be included in Figure 12(c) as 90% dissipation was either not achieved or could not be reliably extrapolated in all cases. As a result, thermal strains will have a prolonged effect on the measured strain profile for large diameter piles during curing. Figures 12b and 12c combined serve as a useful means of estimating the duration of excess hydration temperatures, after which time the thermal strains can be assumed to be due to (the minor) variations in ambient ground temperature only.

As the curing phase is characterised by a reduction in hydration temperature, contraction of the concrete pile would also be expected. However, conflicting strain behaviour during curing was again apparent for the studies in Table 4. Where strains were not corrected from thermal effects (Pennington (1995), Siegel and McGillivray (2009), Fellenius et al. (2009) and Lam and Jefferis (2011)), reported profiles of ε_{total} which trended towards a tensile state as hydration temperatures receded. Plausible reasons noted in the literature for such behaviour include swelling of the pile due to the absorption of moisture from the surrounding soil (Fellenius et al. 2009), drying shrinkage (Hayes and Simmonds 2002) and external restraint from shear stresses acting on the shaft of the pile (Sinnreich, 2012). On the other hand, compressive ε_{mech} profiles which increased with curing time were observed by Farrell and Lawler (2008) and Vipulanandan et al. (2007) for VWSGs. It is clear that the uncertainties regarding the appropriate α-value to apply to the ε_{total} data obtained using VWSGs when correcting for thermal strains has hampered the interpretation of pile behaviour during this phase, leading to conflicting conclusions. Such uncertainties can be eliminated through the use of fibre optics to investigate strain behaviour during curing. In this regard, Kister et al. (2007) reported profiles of ε_{mech} that were compressive, in line with the expected contractile behaviour of a pile undergoing cooling following peak hydration. To date, the use of DFOS during curing of cast-in-situ piles has been primarily limited to thermal profiling (e.g. de Battista et al. 2016; Rui et al. 2017); corresponding measurements of curing strain using this technology are welcomed so as to provide more comprehensive insights in the behaviour of cast-in-situ piles during this phase.

Pile installation and soil consolidation effects

Preformed piles may develop residual loads due to elastic rebound during driving. As already mentioned, downdrag or negative skin friction may arise after pile driving in cohesive soils. These phenomena will occur independently of and in parallel with the processes within the concrete as described above. The development of such residual loads is typically characterised by an increase in compressive strain with time at various sections of the pile, as reported by Siegel and McGillivray

(2009) in CFA piles and Fellenius et al. (2009) in precast post-grouted concrete cylinder piles in soft marine clay after concrete-related effects had diminished. For both studies, the strains near the head of the pile remained relatively constant during this period, which is in general a useful benchmark against which residual load processes elsewhere within the pile can be assessed.

In summary, the effects of the curing process on the development of residual loads in cast-in-situ piles is complicated by the effect of hydration temperatures, particularly in relation to the separation of total and mechanical strains using VWSGs. The various methods for interpreting the magnitude of residual load from these curing strains are critically reviewed by Flynn and McCabe (2021) in the context of curing records.

LOAD TESTING

Following a suitable equalisation or curing period, for which Figure 12 could be used as a guide, an instrumented concrete pile is typically subjected to axial load testing. The predominant type of test used is the maintained compression load test (incorporated in the test programmes of 74% of the case histories in Table 2), with tension and rapid load testing featuring in only 4% and 8% of case histories respectively. The use of bi-directional load tests using an Osterberg cell or 'O-cell' is popular for large diameter bored piles where the size and number of reaction piles otherwise needed becomes cost-prohibitive; these tests arise in 20% of case histories in Table 2.

Test Arrangement

Figure 13a shows the typical arrangement for a static compression load test on an instrumented concrete pile, comprising a hydraulic jack centred over the pile cap which is loaded against a steel reaction frame in turn connected to tension piles using high-strength steel bars. Alternatively, kentledge (e.g. precast concrete blocks or soil) may be utilised to generate the applied load, although this method is falling out of favour due to health and safety concerns, prompted by kentledge failures.

The applied load is measured using a load cell placed between the jack and the reaction frame (Figure 13b), with the pile head displacement determined using linear variable differential transformers (LVDT) connected to an independently-supported reference beam. A minimum of 4 No. LVDTs, orientated at right angles, should be used to capture the effects of rotation of the cap due to eccentricities in the applied load. It is crucial that logging of strain from each gauge during the load test is carried out at the same frequency as the applied load and pile head displacement in order to expedite the strain interpretation process. Further details of static load testing procedures are presented by Bica et al. (2014).

Load schedule

For routine commercial projects, the load schedule for an instrumented load test typically comprises an extended version of that specified for working piles but these can vary considerably from region to region. In the United States, for example, piles are typically tested in accordance with a 'quick' method specified in ASTM D1143 (ASTM, 2020) whereby a series of axial load increments equivalent to 5-10% of the maximum applied load are applied for a maximum hold periods of 15 minutes. In contrast, the Institution of Civil Engineers (ICE) Specification for Piling and Embedded Retaining Walls or SPERW (ICE, 2017), the industry standard method for pile testing in the United Kingdom and Ireland, requires compression loads to be applied in increments corresponding to 10-25% of the pile's specified working load (SWL), with unload-reload cycles performed at SWL and 1.5 × SWL. Furthermore, ICE SPERW specifies minimum hold periods ranging from 10 minutes to 6 hours to permit the effects of concrete creep displacement to be assessed.

To highlight these contrasting load schedules, Figure 14 illustrates a generic example of the applied load variation with elapsed time for a maintained compression load test on a pile with a maximum applied load corresponding to 3.0 × SWL. For a test undertaken in accordance with ASTM D1143, the test duration will be 6 hours, whereas ICE SPERW yields a minimum test duration of over 30 hours (assuming that pile displacements stabilise at the minimum hold period, which is unlikely).

The load test performed in accordance with ICE SPERW will undoubtedly result in a more challenging strain interpretation process due to the effects of creep within the pile during each hold on the measured strains (Lam and Jefferis, 2011), as well as complexities arising from the unload-reload cycles which induce additional residual loads in the pile. As such, performing unload-reload cycles prior to achieving geotechnical pile failure is discouraged (Fellenius, 2020; Fellenius and Ruban, 2020; Siegel 2010).

CONCLUSIONS

This paper provides a detailed review of methodologies employed for the successful execution of an instrumented concrete pile test, including selection of appropriate strain gauges, their arrangement within a pile, issues associated with installation and curing, as well as static load testing. A database of over 100 published case histories on instrumented piles was collated to inform this review. Key takeaway points from the review include the following:

- VWSGs are the dominant gauge type in the literature, although DFOS are becoming more prevalent due to their ability to provide continuous profiles of strain which enhance the interpretation of pile behaviour.
- Four gauges per level at 90º separation should be used to account for the effects of bending during the load test, as well as for redundancy purposes. The use of a one or three gauge strategy per level is discouraged due to the inability of these configurations to compensate for malfunctioning gauges. Two gauges per level may be appropriate as a cost-saving measure at locations away from the head of a pile (where bending effects are greatest). The location of changes in strata should be identified carefully (using continuous profiling) before siting gauges at these levels.
- Plunging of the reinforcement cage after concreting (for CFA and DCIS piles) can result in significant damage to the strain gauge instrumentation due to issues with early-set in concrete, steel congestion and non-verticality.

- In-situ curing results in changes in temperature due to concrete hydration. The time to peak temperature is a function of the pile diameter, whereas the time from peak temperature to the time at which only 10% of excess temperature remains is proportional to the square of the pile diameter. The data presented in this paper enable the duration of the hydration process to be estimated, which is helpful in determining when the load test might be conducted.
- The variations in strain during curing reported in the literature are highly conflicting, primarily due to inconsistencies in the choice of α-value for thermal strain correction in VWSGs.
- Whilst the static load test arrangement is relatively common worldwide, load test schedules vary considerably. Excessive hold durations promote creep displacements which complicate the strain interpretation process. The benefits of unload-reload cycles prior to reaching the maximum pile load are questionable, particularly as these cycles induce additional residual loads which are complex to interpret from the instrumentation.

The companion paper guides the reader through the strain interpretation process using case histories, in light of the challenges highlighted in this paper.

ACKNOWLEDGEMENTS

The authors wish to thank Dr Nicky de Battista of University of Cambridge, Dr Andrew Galbraith of Geowynd, and Drs David Gill and Eric Farrell of AGL Consulting for permission to reuse the various figures referenced in the paper. The first author was sponsored by the College of Engineering and Informatics Fellowship and University Foundation Bursary during his doctoral studies at NUI Galway. The views expressed in this paper are solely the opinions of the authors and do not represent the views of AGL Consulting.

REFERENCES

Abd Elaziz AY and El Naggar MH (2014) Geotechnical capacity of hollow-bar micropiles in cohesive soils. Canadian Geotechnical Journal 51(10): 1123–1138.

Abdlrahem MA and El Naggar MH (2020) Axial performance of micropile groups in cohesionless soil from full-scale tests. Canadian Geotechnical Journal 57(7): 1006–1024.

Abu-Farsakh M, Nafiul Haque M, Tavera E and Zhang Z (2017) Evaluation of pile setup from Osterberg Cell load tests and its cost-benefit analysis. Transportation Research Record: Journal of the Transportation Research Board, 2656, 61–70.

Albuquerque PJR, Carvalho D and Massad F (2005) Bored, continuous flight auger and omega instrumented piles: behavior under compression. In *Proceedings of the 16th International on Soil Mechanics and Geotechnical Engineering, Osaka, Japan*, pp. 2075–2078.

Altee A, Fellenius BH and Evgin E (1992) Axial load transfer for piles in sand. I. Tests on an instrumented precast pile. Canadian Geotechnical Journal 29(1): 11–20.

Amis T, Bourne-Webb P, Davidson C, Amatya B and Soga K (2008) The effects of heating and cooling energy piles under working load at Lambeth College, UK. In *Proceedings of the 11th International Conference on Deep Foundations. New York, USA*.

ASTM (2020) D1143/D1143M–20. Standard test methods for deep foundation elements under static compressive load. ASTM International, West Conshohocken, PA, USA.

Avasarala S, Mummaneni S, Vemula V and Putcha S (2017). Case study: load transfer analysis on an instrumented augercast pile using EDC strain gauges and Geokon rebar strainmeters. In Pr*oceedings of DFI-PFSF Piled Foundations & Ground Improvement Technology for the Modern Building and Infrastructure Sector, Melbourne, Australia*, pp. 356–366.

Axtell PJ, Thompson WR and Brown DA (2009) Drilled shaft foundations for the kcICON Missouri River Bridge. In *Proceedings of the 34th DFI Annual Conference on Deep Foundations, Kansas City, MI, USA*, pp. 3–12.

Ayithi A, Hersbst D and Ryan WG (2016) Inclusion of overburden soils resistance into shaft nominal capacity for significant economic savings – an Osterberg cell load test case study. In *Proceedings of the International Conference on the 41st DFI Annual Conference on Deep Foundations, New York, NY, USA*, pp. 487–496.

Baker C (1991) Prediction and performance of drilled shafts constructed under slurry. In *Proceedings of the 16th DFI Annual Conference, Chicago, Illinois, USA*, pp. 155–172.

Barker C, Niewiarowski M and Patel D (2010) Central Saint Giles – basement and foundations designed for future Crossrail tunnelling. In *Proceedings of the DFI and EFFC 11th International Conference on Geotechnical Challenges in Urban Regeneration, London, UK.*

Batten M, Powrie W, Boorman R and Leiper Q (1999) Use of vibrating wire strain gauges to measure loads in tubular steel props supporting deep retaining walls. Proceedings of the Institution of Civil Engineers – Geotechnical Engineering 137(1): 3–13.

Bersan S, Bergamo O, Palmieri L, Schenato L and Simonini P (2018) Distributed strain measurements in a CFA pile using high spatial resolution fibre optics sensor. Engineering Structures 160: 554–565.

Bica AVD, Prezzi M., Seo H, Salgado R and Kim D (2014) Instrumentation and axial load testing of displacement piles. Proceedings of the Institution of Civil Engineers – Geotechnical Engineering 167(3): 238–252.

Bicocchi N (2011) Structural and geotechnical interpretation of strain gauge data from laterally loaded reinforced concrete piles. PhD thesis. School of Civil Engineering and the Environment, University of Southampton.

Brinkman J, van de Water JG and de Jong E (2009) Large diameter casing piles, design, testing and monitoring. In *Proceedings of the 17th International Conference on Soil Mechanics and Geotechnical Engineering, Alexandria, Egypt*, pp. 1201–1204.

Brown DA (2002) Effect of construction on axial capacity of drilled foundations in Piedmont soils. Journal of Geotechnical and Geonvironmental Engineering 128(12): 967–973.

Brown MJ and Hyde AFL (2008) Rate effects from pile shaft resistance measurements. Canadian Geotechnical Journal 45(3): 425–431.

Brown DA, Muchard M and Khouri B (2002) The effect of drilling fluid on axial capacity, Cape Fear, NC. In *Proceedings of the Deep Foundations Institute 27th Annual Meeting, San Diego, CA, USA*, pp. 1–5.

Buggy F, England M and Fryer S (2019) High-capacity O-cell pile load testing in Coal Measures Mudstone, Northern Spire Bridge, Sunderland U.K. In *Proceedings of the 17th European Conference on Soil Mechanics and Geotechnical Engineering, Reykjavik, Iceland*, pp. 1– 8.

Campbell Scientific (2020) VWIRE 305 8-Channel Dynamic Vibrating-Wire Analyzer Product Manual, Revision 11/2020, Campbell Scientific Inc., USA.

Carvalho D and Albuquerque PJR (2013) Uplift behavior of bored piles in tropical unsaturated sandy soil. In *Proceedings of the 18th International Conference on Soil Mechanics and Geotechnical Engineering, Paris, France*, pp. 2707–2710.

CEN (Comité Européen de Normalisation) (2004) Eurocode 7: Geotechnical Design – Part 1: General Rules. EN 1997-1-2004. CEN, Brussels, Belgium.

Chen CS and Hiew LC (2006) Performance of bored piles with difference construction methods. Proceedings of the Institution of Civil Engineers – Geotechnical Engineering 159(3): 227–232

Chen Q, Nafiul Haue M, Abu-Farsakh M and Fernandez BA (2014) Field investigation of pile setup in mixed soil. Geotechnical Testing Journal 37(2): 1–14.

Choquet P, Juneau F and Dadoun F (1999) New generation of fiber optic sensors for dam monitoring. In *Proceedings of the 99th International Conference on Dam Safety and Monitoring*, China, pp. 1–10.

Cola S, Bersan S, Michielin E, Tchamaleu Pangop F and Simonini, P (2019) On distributed strains in a CFA pile via DFOSs measurements and numerical analysis. In *Proceedings of the 17th European Conference on Soil Mechanics and Geotechnical Engineering*, Reykjavik, Iceland, pp. 1–8.

Cunningham JN, Struedlein AW and Castañeda MA (2011) Uplift micropile load transfer in unsaturated Missoula flood deposits. In *Proceedings of the 36th Annual Conference on Deep Foundations, Boston, MA, USA*, pp. 629–636.

De Battista N and Kechavarzi C (2021) Monitoring of piles and diaphragm walls with distributed fibre optic sensors. In *Piling 2020: Proceedings of the Piling 2020 Conference*, pp. 497–502.

De Battista N, Kechavarzi C, Sea H, Soga K and Pennington S (2016) Distributed fibre optic sensors for measuring strain and temperature of cast-in-situ test piles. In *Proceedings of the International Conference on Smart Infrastructure and Construction*, pp. 21–76.

Doan LV and Lehane BM (2020) Axial capacity of bored piles in very stiff intermediate soils. Canadian Geotechnical Journal 57(9): 1417–1426.

Drbe OFE and El Naggar MH (2015) Axial monotonic and cyclic compression behaviour of hollow-bar micropiles. Canadian Geotechnical Journal 52(4): 426–441.

Dunnicliff J (1988). *Geotechnical instrumentation for monitoring field performance*. John Wiley & Sons, New York, USA.

Erol O, Horoz A and Saglamer A (2005) Socket friction capacity of large diameter drilled shafts in highly weathered rock In: *Proceedings of the 16^th^ International Conference on Soil Mechanics and Foundation Engineering, Osaka, Japan*, 2111–2114.

Farrell ER and Lawler M (2008) CFA pile behaviour in very stiff lodgement till. Proceedings of the Institution of Civil Engineers – Geotechnical Engineering 161(1): 49–57.

Fellenius BH (2002) Determining the true distributions of load in instrumented piles. In *International Deep Foundations Congress, ASCE, Orlando, Florida, USA*, pp: 1455–1470.

Fellenius BH (2020). Basics of Foundation Design. See http://www.fellenius.net (accessed 02/12/2020).

Fellenius BH and Nguyen MH (2013) Large diameter long bored piles in the Mekong delta. International Journal of Geoengineering Case Histories 2(3): 196–207.

Fellenius BH and Nguyen BN (2019) Common mistakes in static loading-test procedures and result analyses. Geotechnical Engineering Journal of the SEAGS & AGSSEA 50(3): 20–31.

Fellenius BH and Ruban T (2020) Analysis of strain-gage records from a static loading test on a CFA pile. DFI Journal 14(1): 39–44.

Fellenius BH and Tan SA (2010) Combination of bidirectional-cell test and conventional head-down test. In *The Art of Foundation Engineering Practice, GSP 198*, pp. 240–259.

Fellenius BH and Tan SA (2012) Analysis of bidirectional-cell tests for Icon Condominiums, Singapore. In *Proceedings of the 9th International Conference on Deep Foundations and Testing – IS Kanazawa, Kanazawa, Japan*, pp. 725–733.

Fellenius BH and Terceros M (2014) Response to load for four different types of bored piles. In *Proceedings of the DFI/EFFC 11th International Conference on Piling and Deep Foundations, Stockholm, Sweden*, pp. 1–21.

Fellenius BH, Kim S-R and Chung S-G (2009) Long-term monitoring of strain in instrumented piles. Journal of Geotechnical and Geoenvironmental Engineering 135(11): 1583–1595.

Flynn KN (2014) Experimental investigations of driven cast-in-situ piles. Ph.D thesis. Department of Civil Engineering, National University of Ireland Galway, Galway, Ireland.

Flynn KN and McCabe BA (2021) Instrumented concrete piles tests – Part 2: strain interpretation. Proceedings of the Institution of Civil Engineers – Geotechnical Engineering. Submitted.

Gajjar RH, Basarkar YC and Dewaikar DM (2005) Analytical and field estimates of shaft resistance in socketed piles: Bandra-Worli Sea Link, Mumbai. In *Proceedings of the 30th Annual Conference on Deep Foundations, Chicago, Illinois, USA*, pp. 303–313.

Galbraith AP (2011) Design and performance of deep foundations in Ireland. Ph.D thesis. Department of Civil, Structural and Environmental Engineering, Trinity College Dublin, Ireland.

Gavin KG, Cadogan D and Casey P (2009) Shaft capacity of continuous flight auger piles in sand. Journal of Geotechnical and Geoenvironmental Engineering 135(6): 790–798.

Gavin KG, Cadogan D and Twomey L (2008) Axial resistance of CFA piles in Dublin Boulder Clay. Proceedings of the Institution of Civil Engineers – Geotechnical Engineering 161(4): 171–180.

Gavin KG, Cadogan D, Tolooiyan A and Casey P (2013) The base resistance of non-displacement piles in sand. Part I: field tests. Proceedings of the Institution of Civil Engineers – Geotechnical Engineering 166(6): 540–548.

Glisic B, Inaudi D and Nan C (2002) Pile monitoring with fibre optic sensors during axial compression, pullout, and flexure tests. Transportation Research Record: Journal of the Transportation Research Board 1808: 11–20.

Gura NP, McGettigan ME and Archabal RA (2007) Engineering foundation support for Las Vegas Strip's tallest hotel casino. In *Proceedings of the 32nd DFI Annual Conference on Deep Foundations, Colorado Springs, CO, USA*, pp. 1–10.

Hai NM and Dao DH (2013) Non-conventional pile loading tests in Vietnam. In *Proceedings of the 18th International Conference on Soil Mechanics and Geotechnical Engineering, Paris, France*, pp. 2747– 2750.

Han J and Ye S-L (2006) A field study on the behavior of a foundation underpinned by micropiles. Canadian Geotechnical Journal 43(1): 30–42.

Hartman JJ and Castelli RJ (2009) Drilled shaft foundations for James River Crossing in Richmond Virginia. In *Contemporary Topics in Deep Foundations, Geotechnical Special Publication No. GSP185, Orlando, FL, USA*, pp. 103–110.

Hayes J and Simmonds T (2002) Interpreting strain measurements from loads tests in bored piles. In *Proceedings of the 9th International Conference on Piling and Deep Foundations, Nice, France.* Deep Foundations Institute, Hawthorne, NJ, USA, pp. 663–669.

Hee I, Dodds A, Talby R, Cushing A and Deakin R (2011) Drilled shaft in strong rock – design, validation, and construction of the Beaharnois Canal Bridge, Autoroute 30 Montreal. In *Proceedings of the 36th DFI Annual Conference on Deep Foundations, Boston, MA, USA*, pp. 379–387.

Holman TP (2009) High capacity micropiles in Wissahickon Schist bedrock. In *Contemporary Topics in Deep Foundations, Geotechnical Special Publication No. GSP185, Orlando, FL, USA*, pp. 103–110.

Holman TP, Papthanasiou Y, Gallagher MJ and Khoury M (2007) Piled raft floats on moraine. In *Proceedings of the 32nd DFI Annual Conference on Deep Foundations, Colorado Springs, CO, USA*, pp. 1–12.

Horvath RG, Schebesch D and Anderson M (1987) Instrumented rock-socketed drill piers, Hamilton General Hospital. In *Proceedings of the 12th DFI Annual Members' Conference, Hamilton, Ontario, Canada*, pp. 91–123.

ICE (2017) *Specification for Piling and Embedded Retaining Walls (SPERW), 3rd Edition*. ICE, London, United Kingdom.

Inaudi D and Glisic B (2008) Overview of fibre optic sensing applications to structural health monitoring. In *Proceedings of the 4th Symposium on Geodesy for Geotechnical and Structural Engineering*, Lisbon, Portugal, pp. 1–10.

Islam MR, Ali MM, Lai M-H, Lim K-S and Ahmad H (2014) Chronology of Fabry-Perot Interferometer fiber-optic sensors and their applications: a review. Sensors 14(4): 7451-7488.

Ismael NF (2001) Axial load tests on bored piles and pile groups in cemented sands. Journal of Geotechnical and Geoenviromental Engineering 127(9): 766–773.

Ismael NF and Farraj K (2014) Analysis of load transfer along large diameter bored piles in very dense sands. In *Proceedings of the 39th DFI Annual Conference on Deep Foundations, Atlanta, GA, USA*, pp. 153–159.

Jacobson JR, Camp WM and Siegel TC (2011) Continuous flight auger piles in the Blue Ridge: a case study using instrumentation in pile design. In *Proceedings of the 36th Annual Conference on Deep Foundations, Boston, MA, USA*, pp. 315–324.

Justason MD, Mullins G, Robertson DT and Knight WF (1998) A comparison of static and statnamic load tests in sand: a case study of the Bayou Chico Bridge in Pensacola, Florida. In *Proceedings of the 7th International Conference & Exhibition on Piling and Deep Foundations, Vienna, Austria*, pp. 187–194.

Kania JG and Katoka Sørensen K (2018) A static pile load test on a bored pile instrumented with distributed fibre optic sensors. In *Proceedings of the International Symposium on Field Measurements in Geomechanics (FMGM 2018), Rio de Janeiro, Brazil*, pp. 1–9.

Kechavarzi C, Soga K, de Battista N, Pelecanos L, Elshafie MZEB and Mair RJ (2016) *Distributed Fibre Optic Sensing for Monitoring Civil Infrastructure – A Practical Guide*. Thomas Telford, UK.

Khan, MK, El Naggar MH and Elkasabgy M (2008) Compression testing and analysis of drilled concrete taped piles in cohesive-friction soil. Canadian Geotechnical Journal 45(3): 377–392.

Kim M-G, Cavusoglu E, O'Neill MW, Roberts T and Yin S (2004) Residual load development in ACIP piles in a bridge foundation. In *Geosupport Conference 2004, Orlando, Florida, USA*, pp. 223–235.

Kim S-R, Chung S-G and Fellenius BH (2011) Distribution of residual load and true shaft resistance for a driven instrumented test pile. Canadian Geotechnical Journal 48(4): 583–598.

Kister G, Winter D, Gebremichael YM, Leighton J, Badcock RA, Tester PD, Krishnamurthy S., Boyle WJO, Grattan KTV and Fernando GF (2007) Methodology and integrity monitoring of foundation concrete piles using Bragg grating optical fibre sensors. Engineering Structures 29: 2048–2055.

Klar A, Bennett PJ, Soga K, Mair RJ, Tester P, Fernie R, St John HD and Torp-Peterson G (2006) Distributed strain measurement for pile foundations. Proceedings of the Institution of Civil Engineers – Geotechnical Engineering 159(3): 135–144.

Kou H-L, Chu J, Guo W and Zhang M-Y (2016) Field study of residual forces developed in pre-stressed high-strength concrete (PHC) pipe piles. Canadian Geotechnical Journal 53(4): 696–707.

Krishnan S and Kai LS (2006) A novel approach to the performance evaluation of driven prestressed concrete piles and bored cast-in-place piles. In *Proceedings of the DFI/EFFC 10th International Conference on Piling and Deep Foundations, Amsterdam, Netherlands*, pp. 718–726.

Krishnendu M (2015) Instrumented pile load tests on ACIP piles for a real estate project in Kolkata – a case study. In *Proceedings of the 6th Conference on Deep Foundation Technologies for Infrastructure Development in India*, pp. 192–201.

Ladd BE (2012) Axial behavior of auger cast piles in inner coastal plain geology. In *Proceedings of the 37th DFI Annual Conference on Deep Foundations, Houston, TX, USA*, pp. 493– 500.

Lam C and Jefferis SA (2011) Critical assessment of pile modulus determination methods. Canadian Geotechnical Journal 48(10): 1433-1448.

Lam C, Jefferis SA, Suckling TP and Troughton VM (2015) Effects of polymer and bentonite support fluids on the performance of bored piles. Soils and Foundations 55(6): 1487–1500.

Lee BH, Kim YH, Oark KS, Eom, JB, Kim MJ, Rho BS and Choi HY (2012) Interferometric fibre optic sensors. Sensors 12(3): 2467–2486.

Lee W, Lee W-J, Lee S-B and Salgado R (2004) Measurement of pile load transfer using the Fiber Bragg Grating sensor system. Canadian Geotechnical Journal 41(6): 1222–1232.

Lehane BM, Pennington S and Clarke S (2003) Jacked end-bearing piles in the soft alluvial sediments of Perth. Australian Geomechanics Journal 38(3): 123-135.

Lehane BM, Schneider JA & Xu X (2005) The UWA-05 method for prediction of axial capacity of driven piles in sand. In *Proceedings of the 1st International Symposium on Frontiers in Offshore Geotechnics, Perth, Australia*, pp. 683-689.

Li B and Ruban AF (2009) Static axial load test on strain gauge instrumented concrete pile. In *Proceedings of GeoHalifax 2009*, pp. 227-233.

Li Q, Struedlein AW and Marinucci A (2017) Axial load transfer of drilled shaft foundations with and without steel casing. DFI Journal 11(1): 13–29.

Lim A, Kwanda A and Rahardjo PP (2013) The study of t-z and q-z curves on bored pile based on the results of instrumented pile load test in medium and stiff clays. In *Proceedings of Pile 2013*, pp. 1–5.

Lin X and Lim RM (2011) Field measurements and predictions of concrete temperatures in large diameter drilled shafts in Hawaii. In *Proceedings of Geo-Frontiers 2011*, pp. 202–211.

Ling Z, Wang W, Wu J, Huang M and Yuan J (2019) Shaft resistance of pre-bored precast piles in Shanghai clay. Proceedings of the Institution of Civil Engineers – Geotechnical Engineering 172(2): 228–242.

Liu J, Zhang Z, Yu F and Yang Q (2013) Termination criteria for jacked precast high-strength prestressed concrete pipe piles. Proceedings of the Institution of Civil Engineers – Geotechnical Engineering 166(3): 268–279.

Marinucci A, Moghaddam RB and NeSmith WM (2021) Full-scale load testing and extraction of augered cast-in-place (ACIP) piles in Central Florida. DFI Journal 15(1): 1–21.

McCabe BA (2002) Experimental investigations of driven pile group behaviour in Belfast soft clay. Ph.D thesis. Department of Civil, Structural and Environmental Engineering, Trinity College Dublin, Ireland.

McCartney JS and Murphy MS (2012) Strain distributions in full-scale energy foundations. DFI Journal 6(2): 26–38.

Mohamad H and Tee BP (2015) Instrumented pile load testing with distributed optical fibre strain sensor. Jurnal Teknologi 77(11): 1–7.

Mohamad H, Soga K and Amatya B (2014) Thermal strain sensing of concrete piles using Brillouin Optical Time Domain Reflectometry. Geotechnical Testing Journal 37(2), 333–346.

Mohamad H, Tee BP, Chong MF and Ang KA (2017) Investigation of shaft friction mechanisms of bored piles through distributed optical fibre strain sensing. In *Proceedings of the 19th International Conference on Soil Mechanics and Foundation Engineering, Seoul, South Korea*, pp. 2829–2932.

Muchard M (2006) Statnamic load testing of high capacity marine foundations. In *Proceedings of the DFI Annual Conference*, 2005.

Muchard M and Farouz E (2009) Broadway Viaduct design phase load test program for post grouted shafts. In *Proceedings of the 34th DFI Annual Conference on Deep Foundations, DFI, Kansas City, MI, USA*, pp. 1–8.

Mullins G, Muchard M and Khouri B (2003) Post grouted drilled shafts: a case history of the PGA Boulevard Bridge Project. In *Proceedings of the 28th DFI Annual Conference on Deep Foundations, Miami Beach, FL, USA*, pp. 57–71.

Muthukkumaran K, Sundaravadivelu R and Gandhi SR (2007) Effect of dredging and axial load on a berthing structure. International Journal of Geoengineering Case Histories 1(2): 73–88.

Nazir R, Moayedi H, Mossallanezad M and Tourtiz A (2014). Appraisal of reliable skin friction variation in a bored pile. Proceedings of the Institution of Civil Engineers – Geotechnical Engineering 168(1): 75–86.

Neville A and Brooks J (1987) *Concrete technology*. Longman Group, Harlow, United Kingdom.

Nguyen MH and Fellenius BH (2015) Bidirectional cell tests on not-grouted and grouted large-diameter bored piles. Journal of Geo-Engineering Sciences 2(3-4): 105–117.

Nguyen MH and Fellenius, BH (2014) Bidirectional-cell tests on two 70m long bored piles in Vietnam. In *GeoInstitute Geo Congress 2014*, pp. 482–496.

Nie R, Leng W, Yang Q and Chen YF (2016) An improved instrumentation method for PHC piles. Proceedings of the Institution of Civil Engineers – Geotechnical Engineering 169(6): 494–508.

Omer JR (1998) Numerical analysis of test pile data from instrumented large diameter bored piles formed in Keuper Marl (Mercia Mudstone). PhD thesis. Department of Civil Engineering, University of Glamorgan.

Patel D, Glover S, Chew J and Austin J (2010a) The Pinnacle – design and construction of large diameter deep base grouted piles in London. In *Proceedings of the DFI and EFFC 11th International Conference on Geotechnical Challenges in Urban Regeneration, London, UK*.

Patel D, Williamson M, Troughton V and Pennington M (2010b) Instrumented underream pile test in London Clay constructed using new Stent underream tool. In *Proceedings of the DFI and EFFC 11th International Conference on Geotechnical Challenges in Urban Regeneration, London, UK*.

Pelacanos L, Soga K, Chunge MPM, Ouyong Y, Kwan V, Kechavarzi C and Nicholson D (2017) Distributed fibre-optic monitoring of an Osterberg-cell pile test in London. Géotechnique Letters 7(2): 152–160.

Pelecanos L, Soga K, Elshafie MZ, De Battista N, Kechavarzi C, Gue CY, Ouyang Y and Seo HJ (2018) Distributed fiber optic sensing of axially loaded bored piles. Journal of Geotechnical and Geoenvironmental Engineering: 144(3), 04017122-1 to 16.

Pennington DS (1995) Cracked? Exploring post-construction evidence in the interpretation of trial pile data. Proceedings of the Institution of Civil Engineers – Geotechnical Engineering 113(2): 132–143.

Poulos HG and Davids AJ (2005) Foundation design for the Emirates Twin Towers, Dubai. Canadian Geotechnical Journal 42(3): 716–730.

Puller DJ, Corbet SP and Patterson D (2002) Design of bored piles in chalk at the new Medway crossing based on instrumented load tests. In *Proceedings of the 9th International Conference on Piling and Deep Foundations, Nice, France*, pp. 569–573.

Rabab'ah SR, Niedzielski JC, Elsayed AA, al Bodour W and Durkee DB (2011) Comparison of drilled shaft design methods for drilled shafts in sand, coarse gravel and cobble soils. In *Geo-Frontiers Congress 2011*, *Dallas, Texas, USA*, pp. 212–221.

Raja Shoib RSMS, Rashid ASA and Armaghani DJ (2017) Shaft resistance of bored piles socketed in Malaysian granite. Proceedings of the Institution of Civil Engineers – Geotechnical Engineering 170(4): 335–352.

Rangel J-L, Ibarra E and Mendoza M (2019) A case history on evolution of shaft resistance in long piles placed in layered soils. In *Proceedings of the 16th Pan-American Conference on Soil Mechanics and Geotechnical Engineering (XVI PCSMGE)*, pp. 952–960.

Riker RE and Fellenius BH (1992) A comparison of static and dynamic pile test results. In *Proceedings of the 4th International Conference on the Application of Stress-Wave Theory of Piles*, pp. 143–152.

Robertson DT and Muchard MK (2007) Statnamic load testing of large diameter piles at Rigolets Pass Bridge replacement project. In *Contemporary Issues in Deep Foundations, Geotechnical Special Publication No. GSP158, ASCE, Renton, VA, USA*.

Rocher-Lacoste F, Bustamante M and England M (2009) Bi-directional instrumented load test of a pile bored in Guinea Bissau. In *Proceedings of the 5th International Symposium on Deep Foundations on Bored and Augered Piles, Ghent, Belgium*, pp. 263–268.

Rui Y, Kechavarzi C, O'Leary F, Baker C, Nicholson D and Soga K (2017) Integrity testing of pile cover using distributed fibre optic sensing. Sensors 17(12): 2949.

Russo G (2004) Full-scale load tests on instrumented micropiles. Proceedings of the Institution of Civil Engineers – Geotechnical Engineering 157(3): 127–135.

Sahajda K (2013) Nonlinearity of concrete modulus and its influence on the interpretation of instrumented pile load tests. In *Proceedings of the Conference on Concrete Structures in Urban Areas, Wroclaw, Poland*, pp. 1–10.

Saglamer A, Elif Y, Muge I and Orhan I (2001) Load test on a large diameter instrumented bored pile. In *Proceedings of the 15th International Conference on Soil Mechanics and Geotechnical Engineering, Istanbul, Turkey*, pp. 999–1002.

Safaqah O, Bittner R and Zhang X (2007) Post-grouting of drilled shaft tips on the Sutong Bridge: a case history. In *Contemporary Issues in Deep Foundations, Geotechnical Special Publication No. GSP158, ASCE, Renton, VA, USA*.

Schilder C, Kohlhoff H, Hofmann D, Basedau F, Habel WR, Baeßler M, Niederleithinger E, Georgi S and Herten M (2013) Static and dynamic pile testing of reinforced concrete piles with structure integrated fibre optic strain sensors. In *Proceedings of the 5th European Workshop on Optical Fibre Sensors, Krakow, Poland*, pp. 1–4.

Selemetas D and Standing JR (2017) Response of full-scale piles to EPBM tunnelling in London Clay. Géotechnique 67(9): 823–836.

Seo H, Prezzi M and Salgado R (2013) Instrumented static load test on rock-socketed micropile. Journal of Geotechnical and Geoenvironmental Engineering 139(12): 2037–2047.

Shahien MM and El Naggar HM (2015) Analysis of three axial load tests on large bored grouted deep foundations. In *Proceedings of the 40th DFI Annual Conference on Deep Foundations, Oakland, CA, USA*, pp. 311–320.

Siegel TC (2010) Load testing and interpretation of instrumented augered cast-in-place piles. DFI Journal 4(2): 65–71.

Siegel TC and McGillivray A (2009) Interpreted residual load in an augered cast-in-place pile. In *Proceedings of the Deep Foundations Institute Annual Conference, Kansas City, MO, USA*, pp. 1–10.

Sinnreich J (2012) Strain gage analysis for nonlinear pile stiffness. Geotechnical Testing Journal 35(2), GTJ103412.

Sinnreich J (2021) Optimizing the arrangement of strain gauges in pile load testing. Geotechnical Testing Journal 44(5), GTJ20200033.

Soga K and Luo L (2018) Distributed fibre optics sensors for civil engineering infrastructure sensing. Journal of Structural Integrity and Maintenance 3(1): 1–21.

Sun Y, Li X, Ren C, Xu H and Han A (2020) Distributed fibre optic sensing and data processing of axial loaded precast piles. IEEE Access 8, 169136–169145.

Unwin H and Jessep RA (2004) Long-term pile testing in London Clay: a case study. Proceedings of the Institution of Civil Engineers – Geotechnical Engineering 157(1): 57–63.

Vanderpool WE, Chesnut RL and McGettigan ME (2011) Geotechnical exploration phase drilled shaft load testing. DFI Journal 5(2): 16–22.

Vipulanandan C, Guvener O and McClelland M (2007) Monitoring the installation and curing of a large diameter ACIP pile in very dense sand. In *Contemporary Issues in Deep Foundations, Geotechnical Special Publication No. GSP158, ASCE, Renton, VA, USA*.

Vipulanandan C, Vembu K and Brettmann T (2009) Load displacement behavior of ACIP piles in cohesive soils. In *Contemporary Topics in Deep Foundations, Geotechnical Special Publication No. GSP185, Orlando, FL, USA*, pp. 103–110.

Vipulanandan C, Vembu K and Guvener O (2012) Monitoring auger cast in place pile construction and testing in hard clay. In *Proceedings of the 37th DFI Annual Conference on Deep Foundations, Houston, TX, USA*, pp. 67–76.

Von Rosenvinge T and Beeks B (2011) Deep drilled shafts for the Pearl Harbor Memorial Bridge New Haven, Connecticut, USA. In: *Proceedings of the DFI 36th Annual Conference on Deep Foundations, 2011, Boston, MA, USA*, pp. 255–271.

Walter DJ, Burwash WJ and Montgomery RA (1997) Design of large-diameter drilled shafts for the Northumberland Strait bridge project. Canadian Geotechnical Journal 34(4): 580–587.

Wang Y, Sang S, Zhang M, Bai Z and Su L (2021) Investigation on in-situ test of penetration characteristics of open and closed PHC pipe piles. Soils and Foundations, In press, displacehttps://doi.org/10.1016/j.sandf.2021.06.003

Webb GC and Viswanathan R (2005) Innovative use of ACIP piles and geogrid to support Kroger Superstore. I: *Proceedings of the Augered Cast-In-Place Pile Seminar, Cincinnati, OH, USA*, pp. 97–111.

Wilkinson PD and Butterworth CS (2006) Report on an instrumented continuous flight auger test pile at Ascot. In *Proceedings of the DFI/EFFC 10th International Conference on Piling and Deep Foundations, Amsterdam, The Netherlands*, pp. 790–795.

Zeni L, Picarelli L, Avolio B, Coscetta A, Papa R, Zeni G, Di Maio C, Vassallo R and Minardo A (2015) Brillouin optical time-domain analysis for geotechnical monitoring. Journal of Rock Mechanics and Geotechnical Engineering 7(4): 458–462.

Zhan C and Yin J-H (2000) Field static load tests on drilled shaft founded on or socketed into rock. Canadian Geotechnical Journal 37(6): 1283–1294.

Notation

A_{pile} = pile cross-sectional area

D = pile diameter

E_{pile} = pile modulus

EA = axial rigidity

GF_{ER} = electrical resistance gauge factor

GF_{VW} = vibrating wire gauge factor

P = load

R_0 = initial resistance

T = temperature

$T_{ambient}$ = ambient temperature

T_{peak} = peak temperature

f_0 = initial frequency

f_1 = current frequency

t_{peak} = time to peak hydration temperature

t_{90} = time for 90% dissipation of temperature from T_{peak} to $T_{ambient}$

α = coefficient of thermal expansion

ΔR = change in resistance

ΔT = change in temperature

$\Delta\lambda_B$ = change in Bragg wavelength

λ_B = Bragg wavelength

$\varepsilon_{elastic}$ = elastic strain

ε_{mech} = mechanical strain

$\varepsilon_{thermal}$ = thermal strain

ε_{total} = total (measured) strain

List of Table Captions

List of Figure Captions

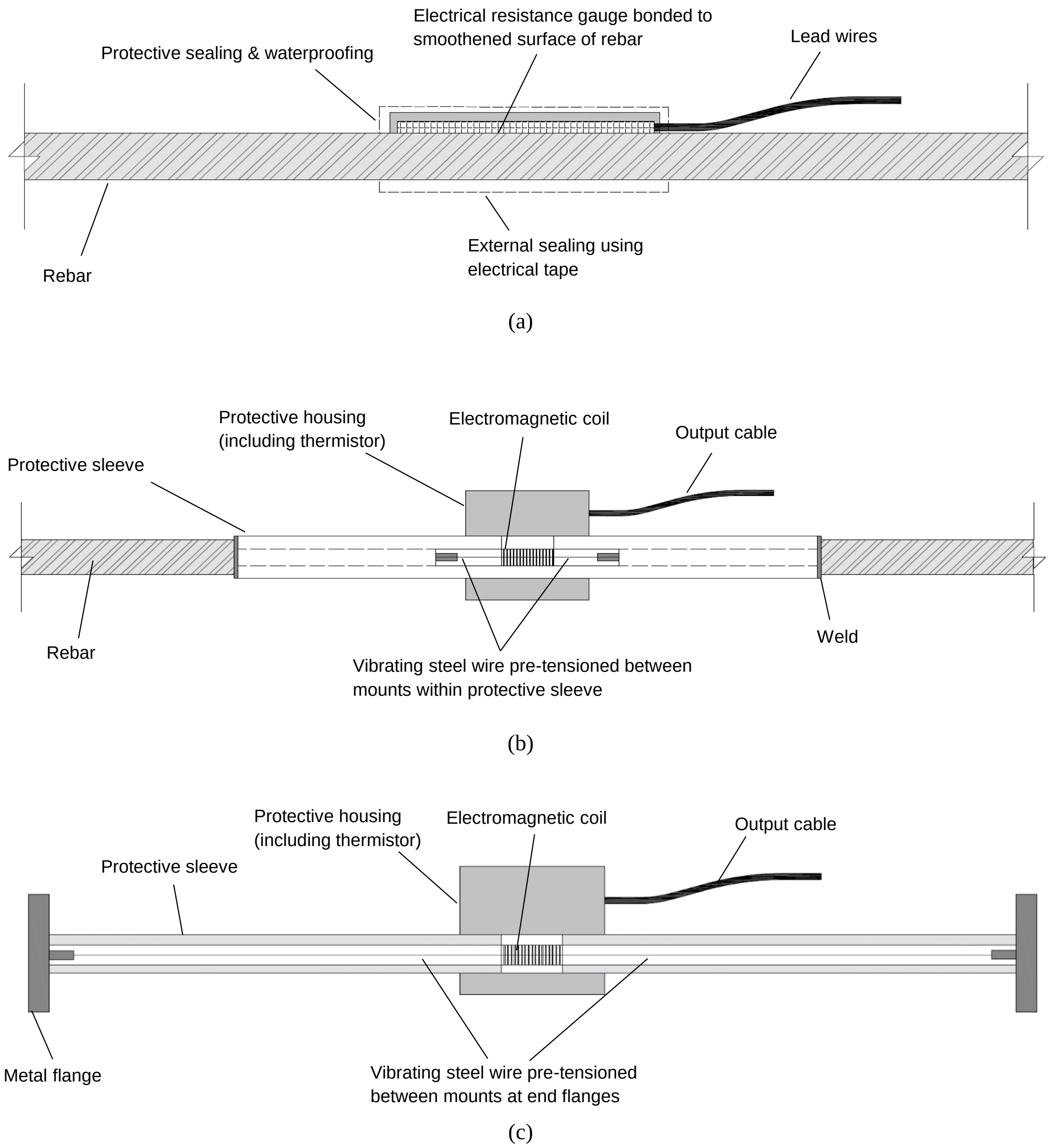

Figure 1. Schematic of (a) bonded foil electrical resistance strain gauge, (b) vibrating wire sister bar and (c) vibrating wire embedment strain gauge

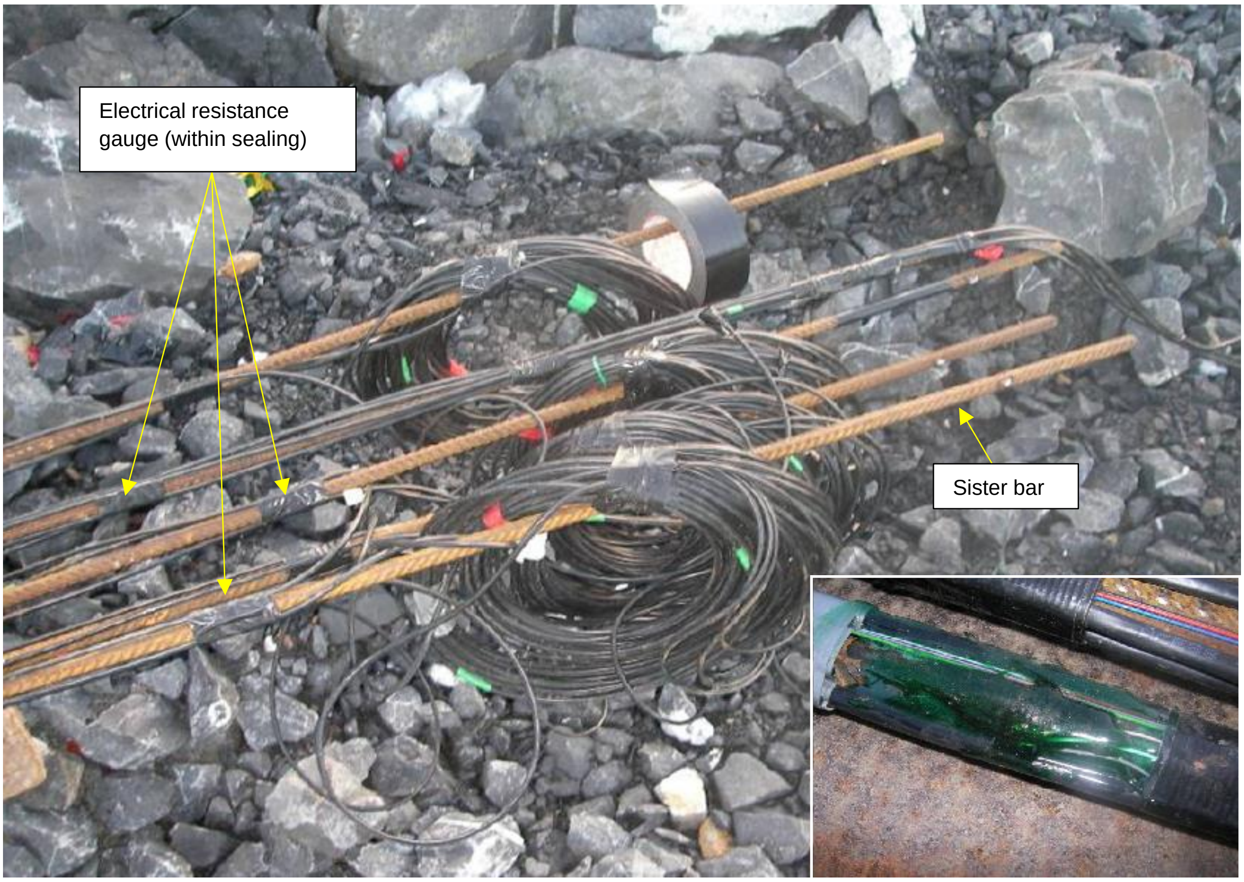

Figure 2. Electrical resistance strain gauges mounted on sister bars (protective sealing shown in inset) (reproduced with permission from Galbraith, 2011)

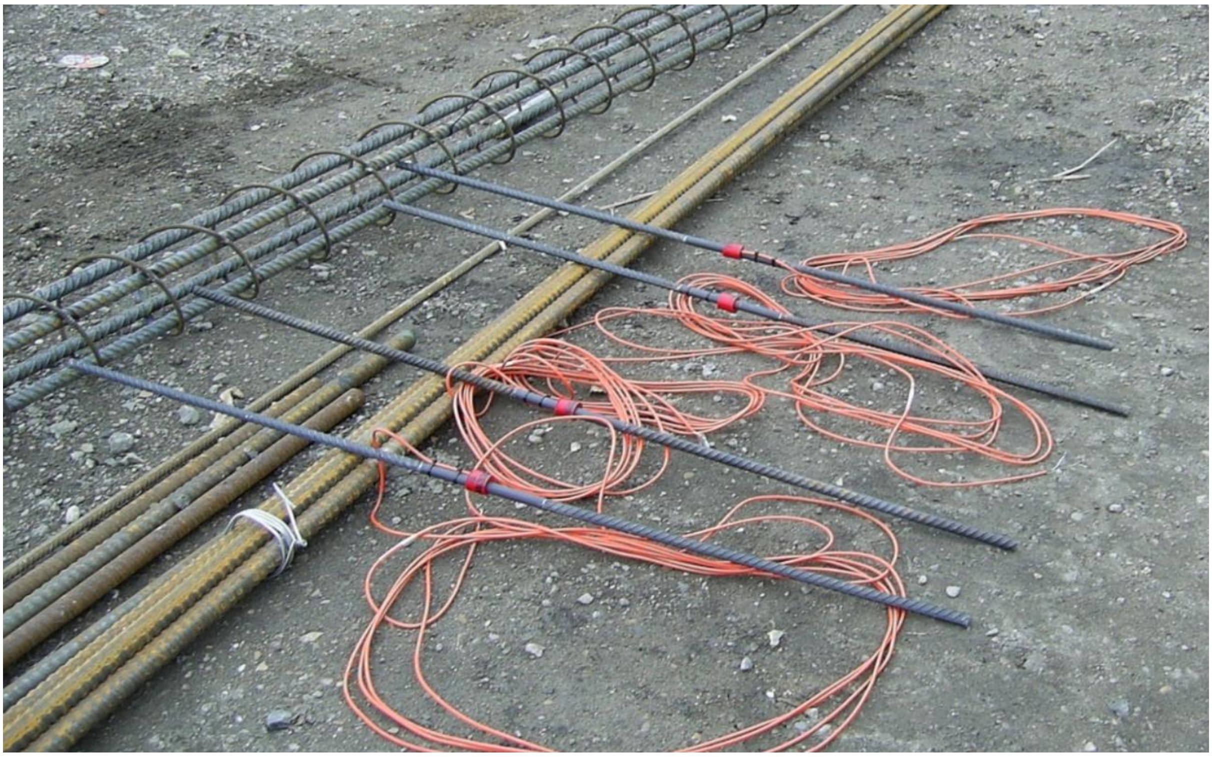

(a)

(b)

Figure 3. Vibrating wire strain (a) standard sister bar gauges and (b) reduced-length sister bar with flanges

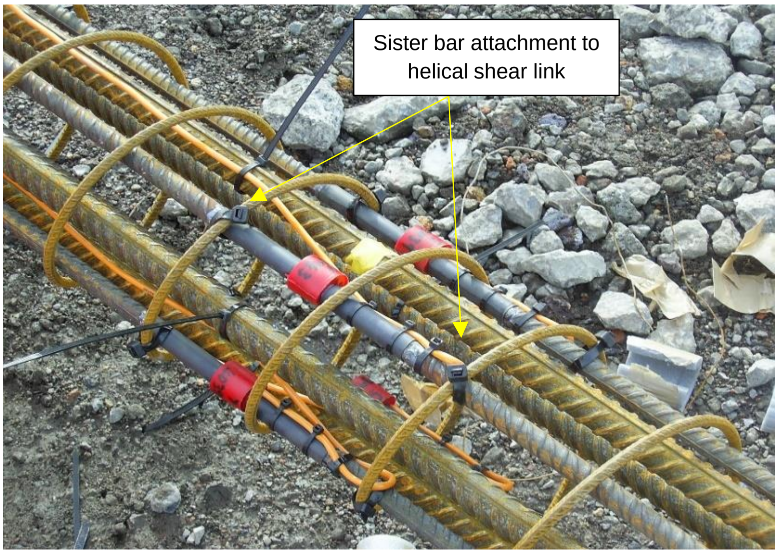

(a)

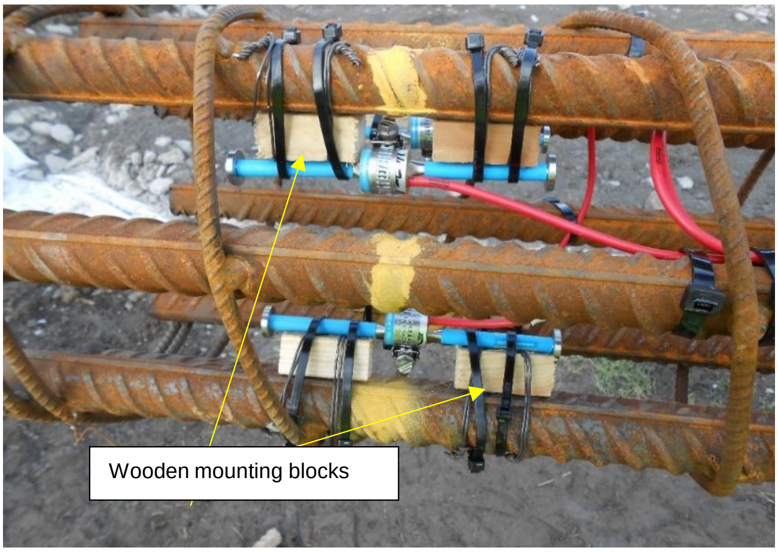

(b)

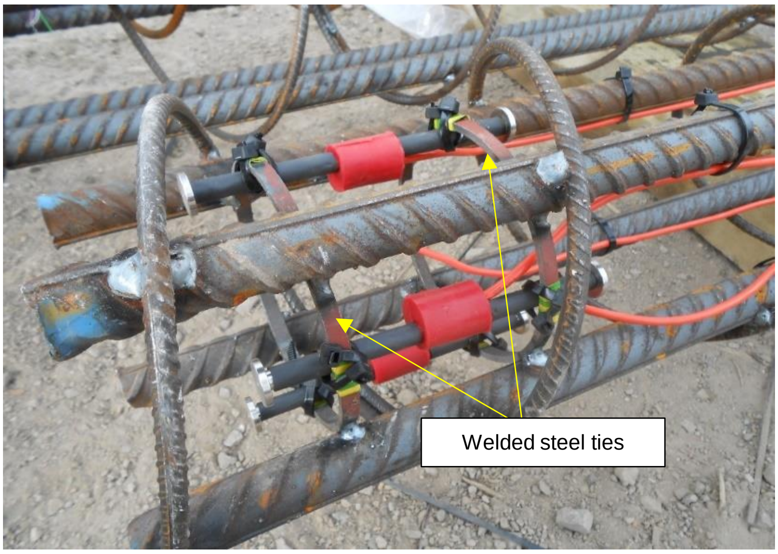

(c)

Figure 4. Typical attachment details for vibrating wire (a) sister bars, (b) embedment gauges using wooden mounts and (b) embedment gauges using welded steel ties

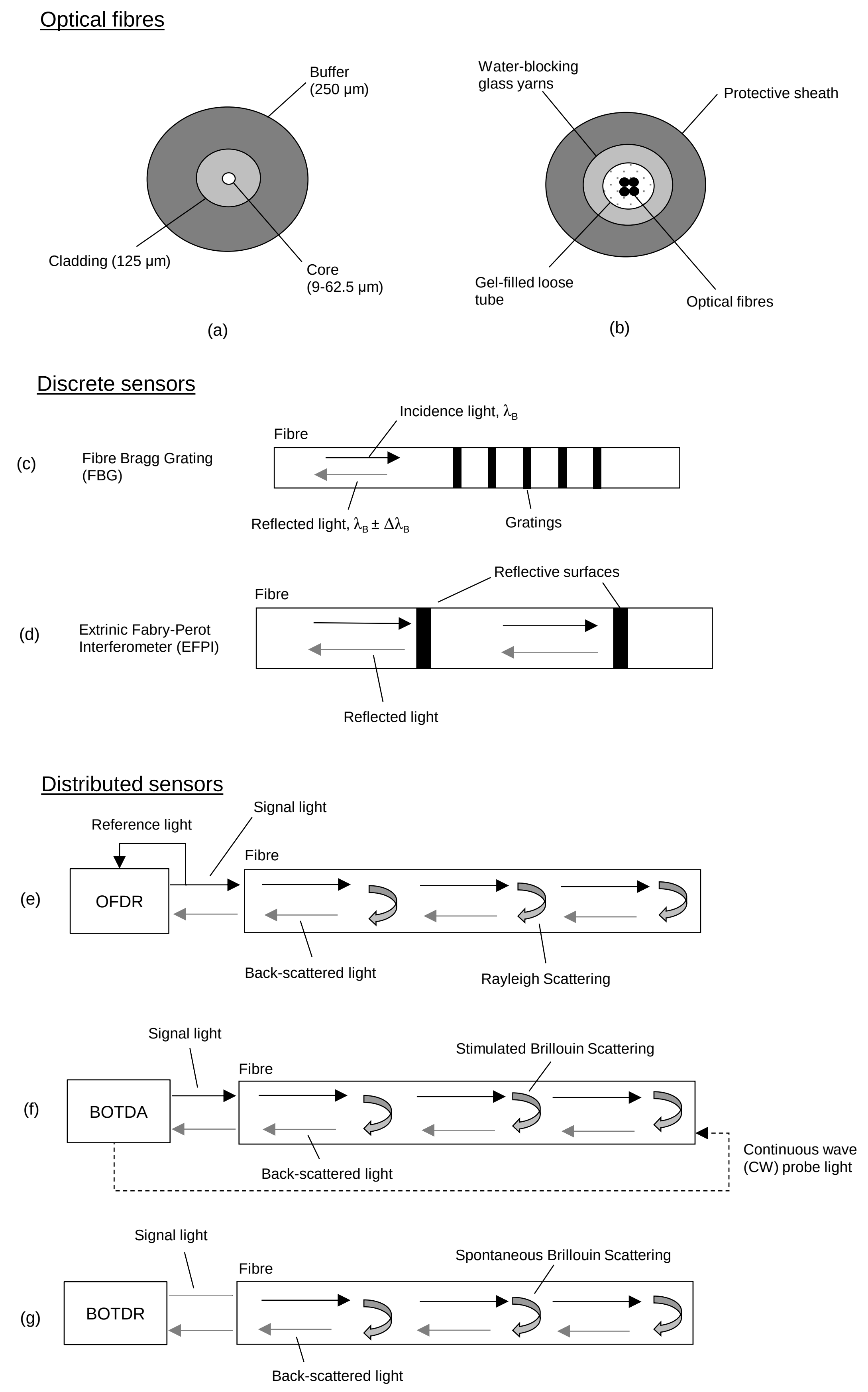

Figure 5. (a) Typical optical fibre structure, (b) temperature sensing fibre optic cable, (c) fibre Bragg grating, (d) extrinsic Fabry-Perot Interferometer, (e) Optical Frequency-Domain Reflectometry, (f) Brillouin Optical Time-Domain Analysis and (g) Brillouin Optical Time-Domain Reflectometry

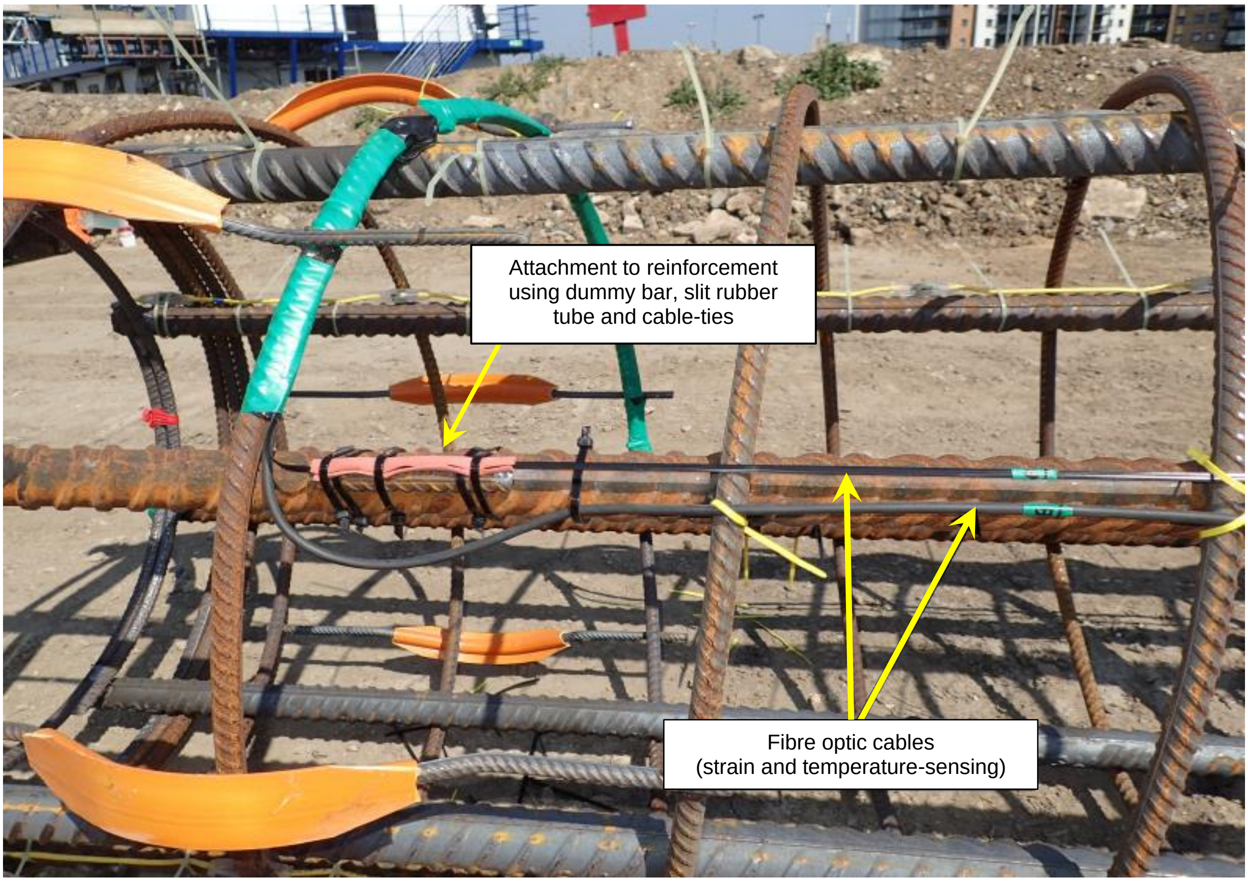

Figure 6. Distributed fibre optic sensor cables (reproduced with permission from de Battista et al. 2016)

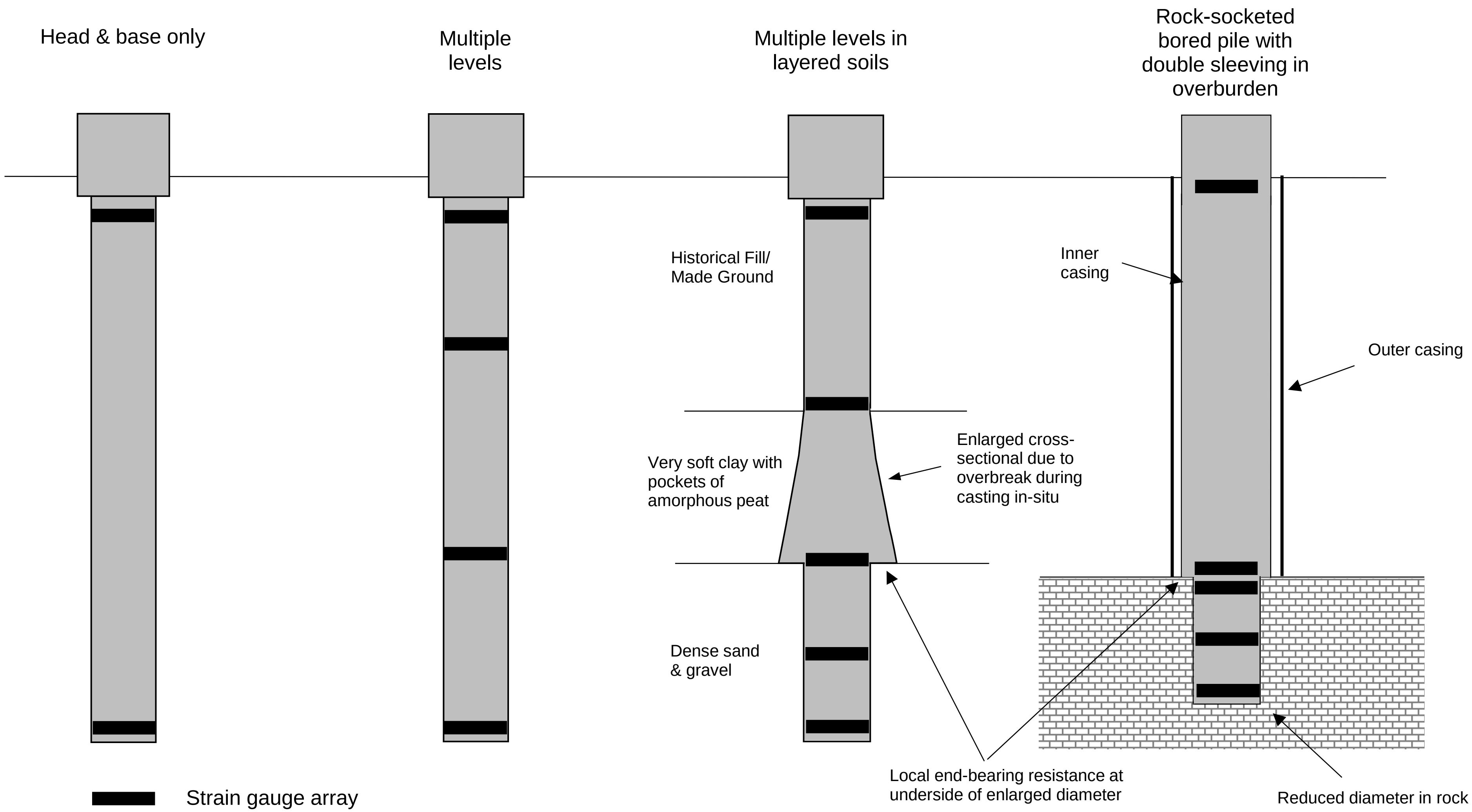

Figure 7. Examples of typical strain gauge levels

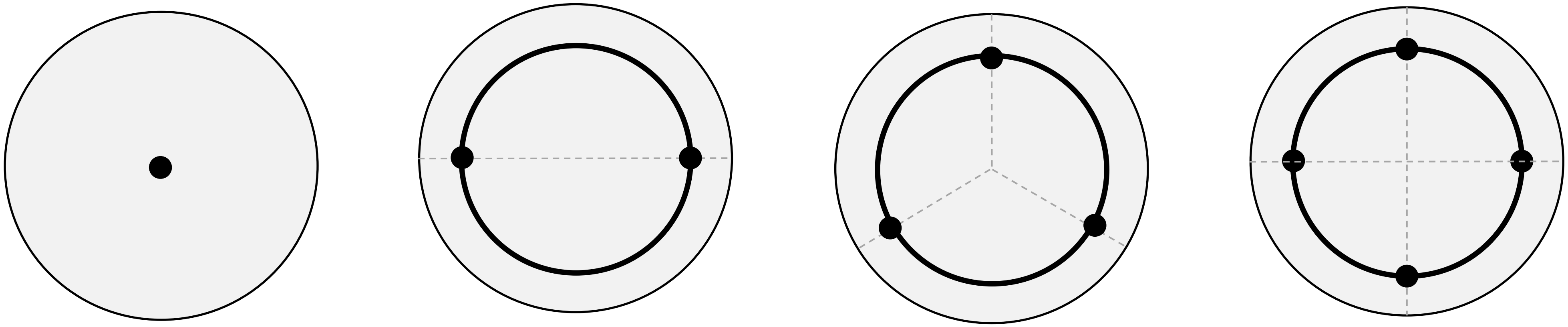

(a) (b) (c) (d)

Figure 8. Typical strain instrumentation arrangements – (a) 1 No. central, (b) 2 No. at 180^o, (c) 3 No. at 120^o and (d) 4 No. at 90^o

(a)

(b)

Figure 9. Pile test cap configurations – (a) circular and (b) square

(a) (b)

Figure 10. (a) Installation of double pile sleeve to minimise shaft resistance and (b) use of a polystyrene to create a soft toe ((reproduced with permission from Drs David Gill and Eric Farrell, AGL Consulting)

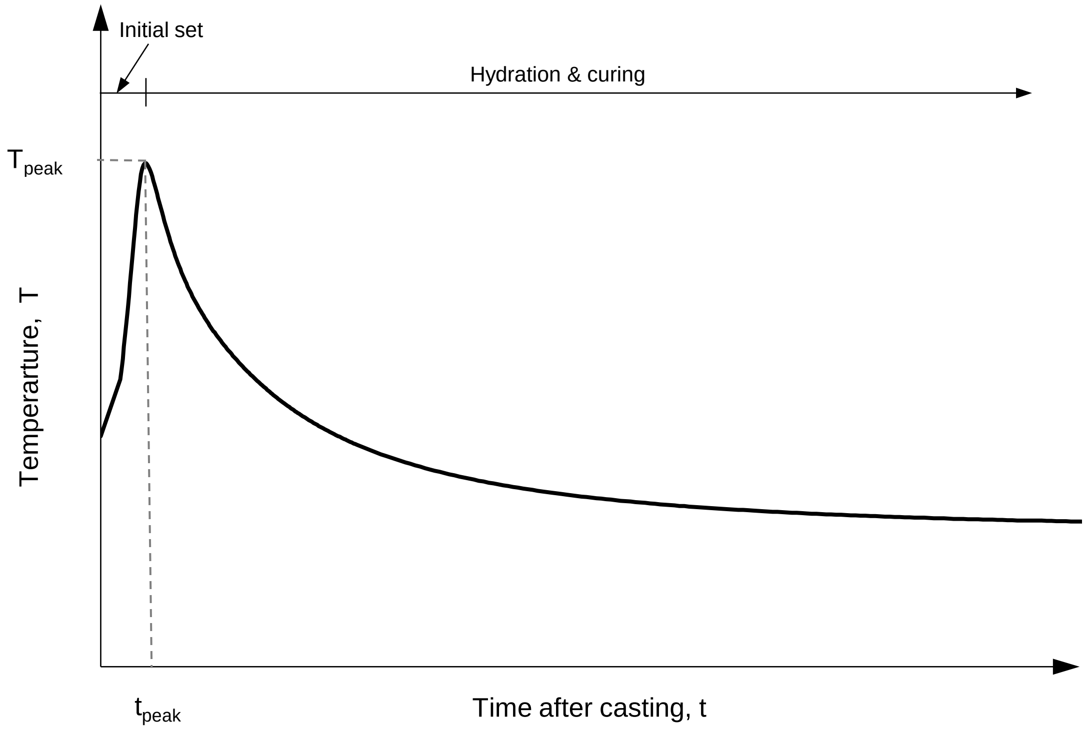

(a)

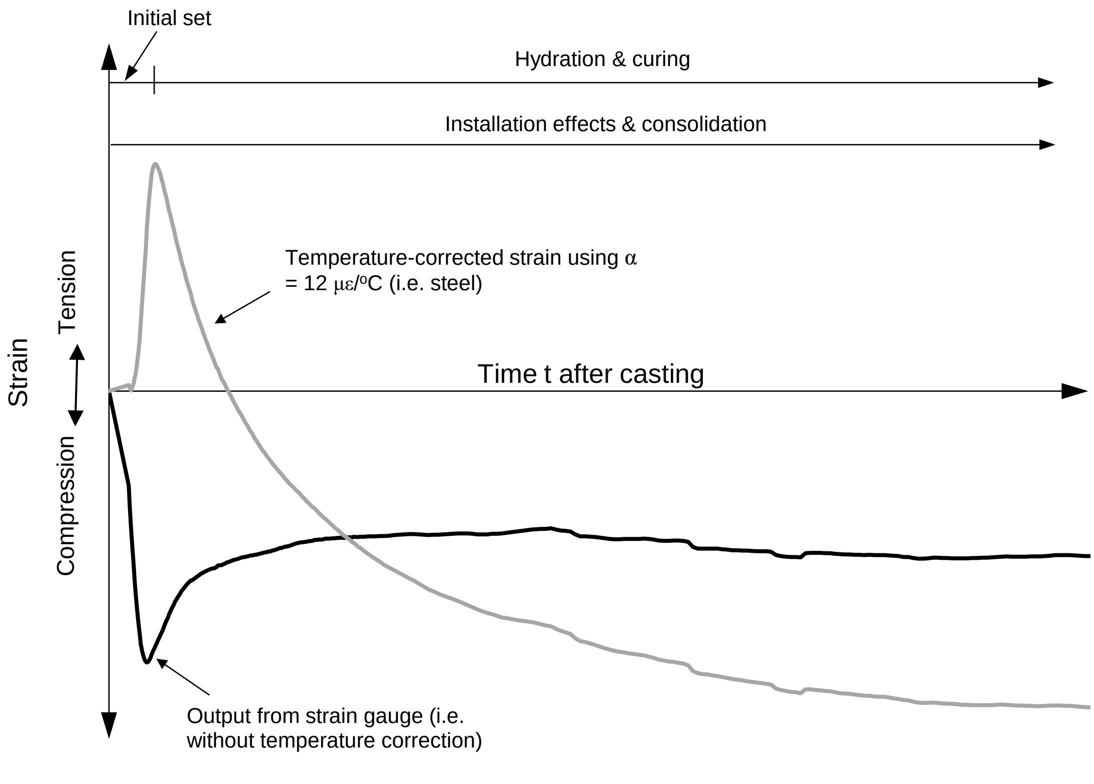

(b)

Figure 11. Variation with time after casting of (a) temperature and (b) strain for cast-in-situ concrete piles

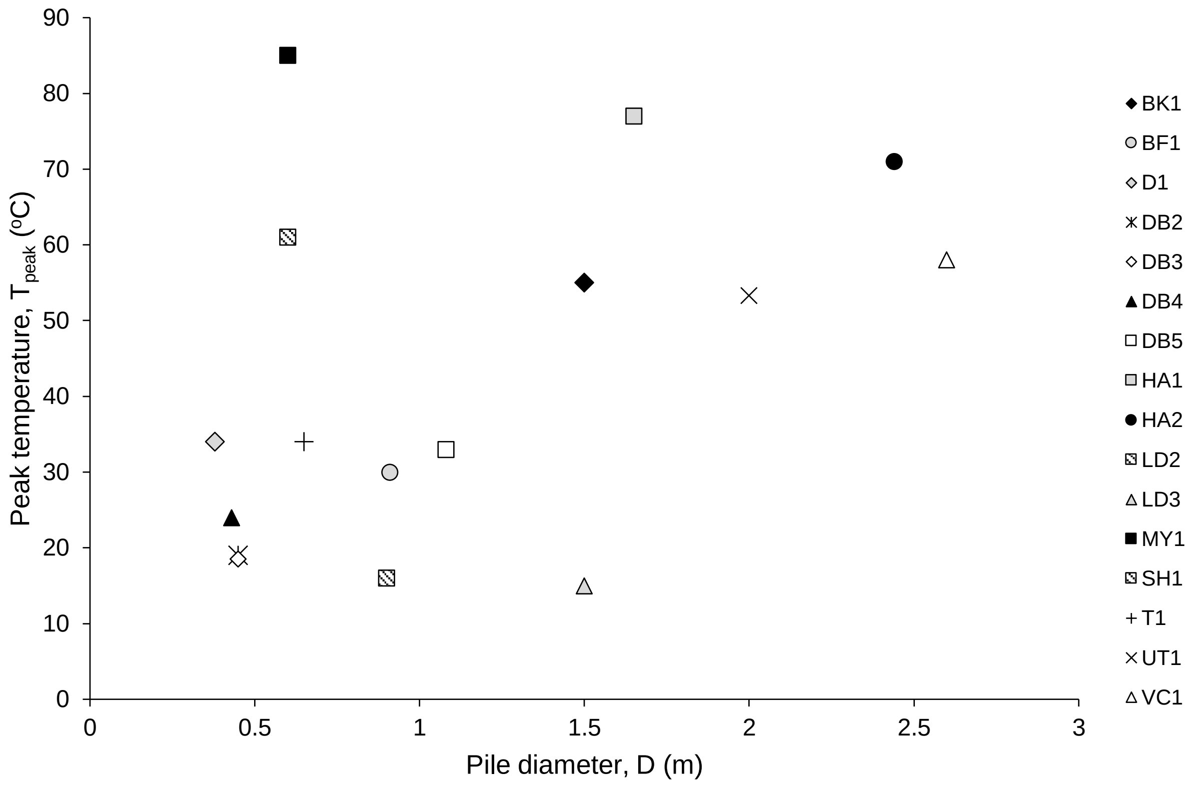

(a)

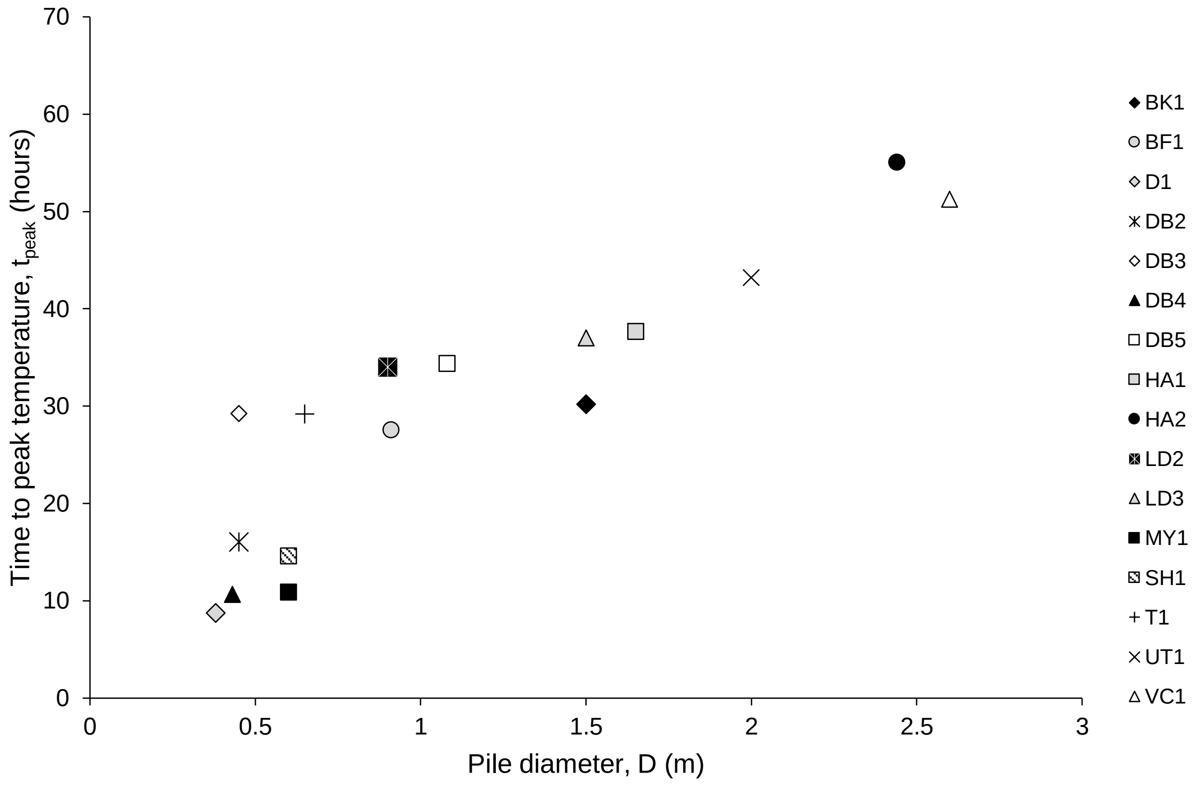

(b)

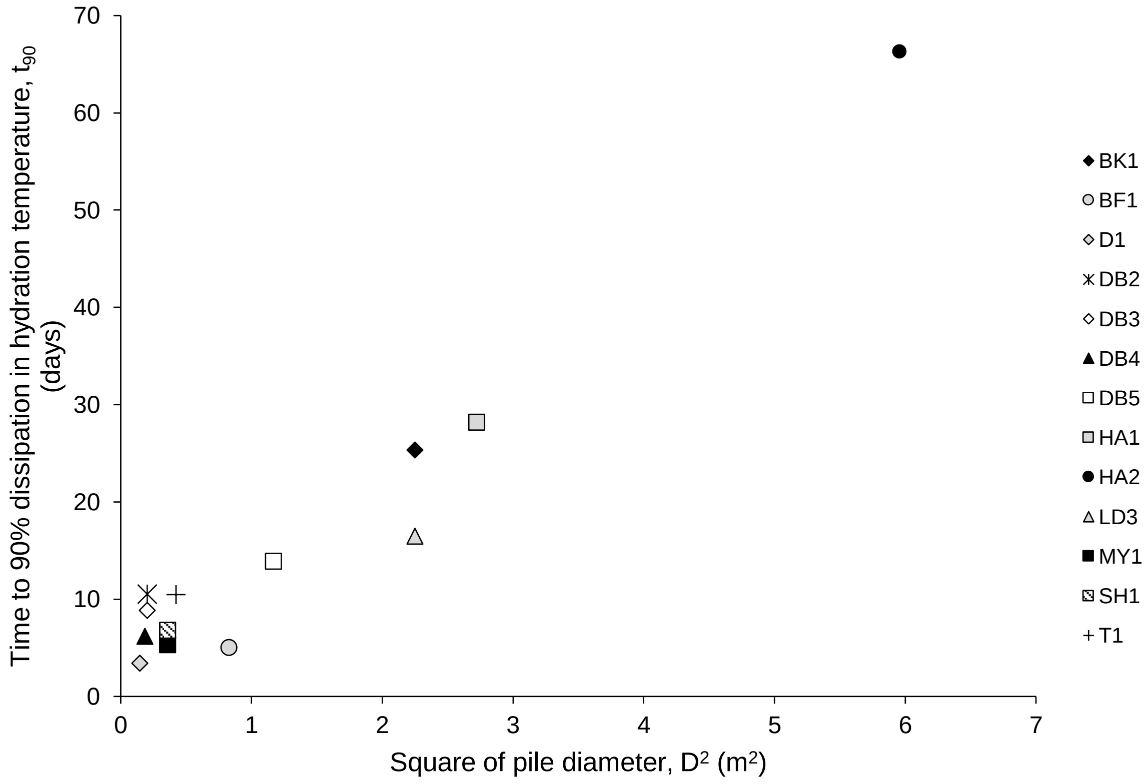

(c)

Figure 12. Variation with pile shaft diameter of (a) peak temperature, (b) time to peak temperature and (c) time between peak and 10% excess temperature - see Table 4 for legend reference

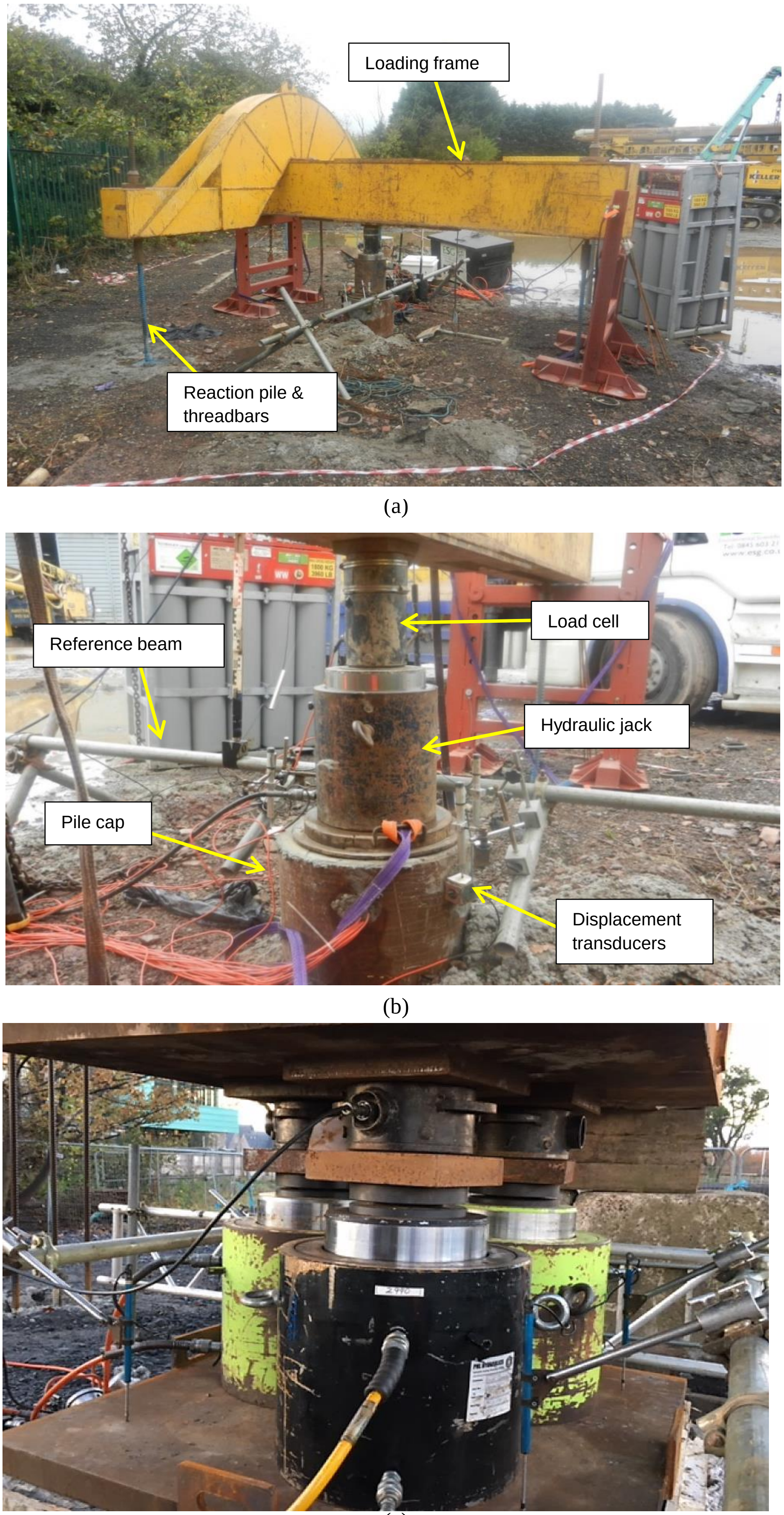

Figure 13. Typical arrangement for (a) static load test with reaction piles, (b) load test instrumentation and (c) multiple hydraulic jacks

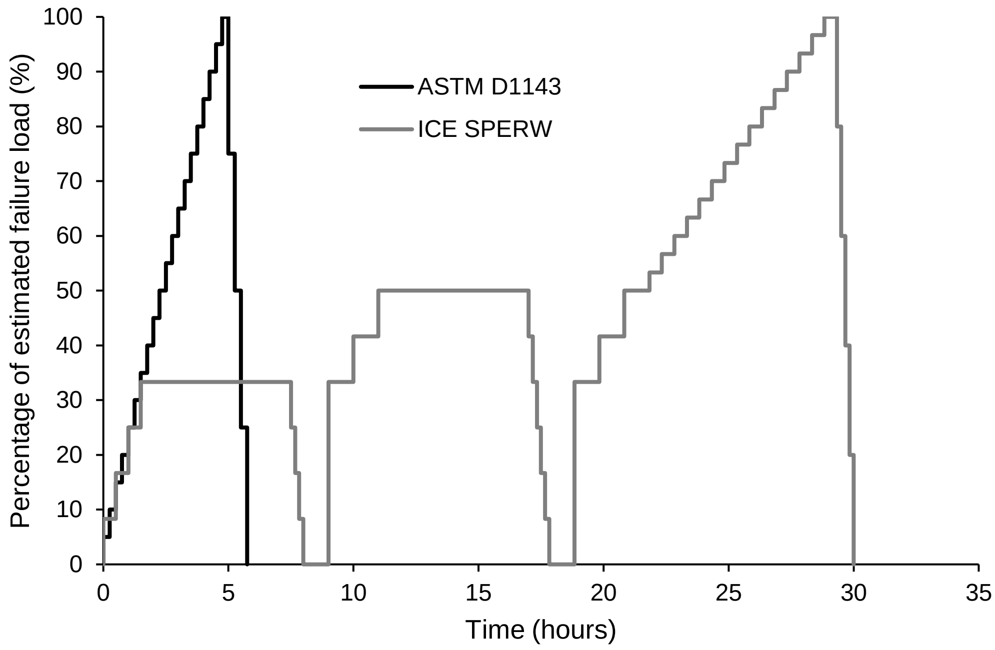

Figure 14. Comparison of load schedules specified by ASTM D1143 and ICE SPERW